

1 **Short summary.** Wolverine denning habitat inferred using a snow threshold differed for three different spatial
2 representations of snow. These differences were ~~annually repeatable and~~ based on the annual volume of snow and
3 the elevation of the snow line. While denning habitat was most influenced by winter meteorological conditions, our
4 results show that studies applying thresholds to environmental datasets should report uncertainties stemming from
5 different spatial resolutions and uncertainties introduced by the thresholds themselves.

6 **Interactions between thresholds and spatial discretizations of snow: insights** 7 **from estimates of wolverine denning habitat ~~wolverine habitat assessments in~~** 8 **the Colorado Rocky Mountains**

9 Justin M. Pflug^{1,a,b}, Yiwen Fang², Steven A. Margulis², Ben Livneh^{1,3}

10 ¹Cooperative Institute for Research in Environmental Science (CIRES), University of Colorado,
11 Boulder, CO, 80309, USA

12 ²Department of Civil and Environmental Engineering, University of California, Los Angeles, CA,
13 90095, USA

14 ³Department of Civil, Environmental and Architectural Engineering, University of Colorado, Boulder,
15 CO, 80309, USA

16 ^anow at: Hydrological Sciences Laboratory, NASA Goddard Space Flight Center, Greenbelt, MD,
17 20771, USA

18 ^bnow at: ESSIC, University of Maryland, College Park, College Park, MD, 20742, USA

19 *Correspondence to:* Justin M. Pflug (jpflug@umd.edu)

20 **Abstract.** Thresholds can be used to interpret environmental data in a way that is easily communicated and useful
21 for decision making purposes. However, thresholds are often developed for specific data products and time periods,
22 changing findings when the same threshold is applied to datasets or periods with different characteristics. Here, we
23 test the impact of different spatial discretizations of snow on annual estimates of wolverine denning
24 ~~opportunities habitat~~ in the Colorado Rocky Mountains, defined using a snow water equivalent (SWE) threshold
25 (0.20 m) and threshold date (15 May) from previous habitat assessments. Annual potential wolverine
26 ~~denning habitable area (PWDA) (WHA)~~ was thresholded from a 36-year (1985 – 2020) snow reanalysis ~~model with~~
27 three different spatial discretizations: 1) 480 m grid cells (D480), 2) 90 m grid cells (D90), and 3) 480 m grid cells
28 with implicit representations of subgrid snow spatial heterogeneity (S480). Relative to the D480 and S480
29 ~~discretizations 480 m grid cells, D90 90 m grid cells~~ resolved shallower snow deposits on slopes between 3050 and
30 3350 m elevation, decreasing PWDA-WHA by 10%, on average. In years with warmer and/or drier winters, S480
31 ~~discretizations with subgrid representations of snow heterogeneity grid cells with subgrid representations of snow~~
32 ~~heterogeneity~~ increased the prevalence of 15 May snow deposits that exceeded the 0.20 m SWE threshold PWDA,
33 even within grid cells where mean 15 May SWE was less than the SWE threshold. These simulations increased
34 PWDA-WHA by upwards of 30% in low snow years, as compared to the D480 and D90 simulations without subgrid
35 snow heterogeneity. Despite PWDA-WHA sensitivity to different snow spatial discretizations, PWDA-WHA was
36 controlled more by annual variations in winter precipitation and temperature. However, small changes to the SWE
37 threshold (± 0.07 m) and threshold date (± 2 weeks) also affected PWDA-WHA by as much as 82%. Across these
38 threshold ranges, PWDA-WHA was approximately 18% more sensitive to the SWE threshold than the threshold date.
39 However, the sensitivity to the threshold date was larger in years with late spring snowfall, when PWDA-WHA
40 ~~depended greatly on~~ depended on whether ~~modeled the date~~ SWE was thresholded ~~was~~ before, during, or after spring
41 snow accumulation. Our results demonstrate that snow thresholds are useful but may not always provide a complete
42 picture of the annual variability in snow-adapted wildlife denning opportunities habitat. Studies thresholding
43 spatiotemporal datasets could be improved by including 1) information about the fidelity of thresholds across
44 multiple spatial discretizations, and 2) uncertainties related to ranges of realistic thresholds.

45 **1. Introduction**

46 Generalizing environmental data using thresholds can present information in a way that is more easily understood,
47 communicated, and applied for decision-making purposes. Conceptually, thresholds are static constraints intended to
48 partition the areas, timing, and/or prevalence of data greater or less than some scientifically or managerially relevant
49 limit. In the field of snow science, thresholds are used to classify snow cover and snow absence from remotely-

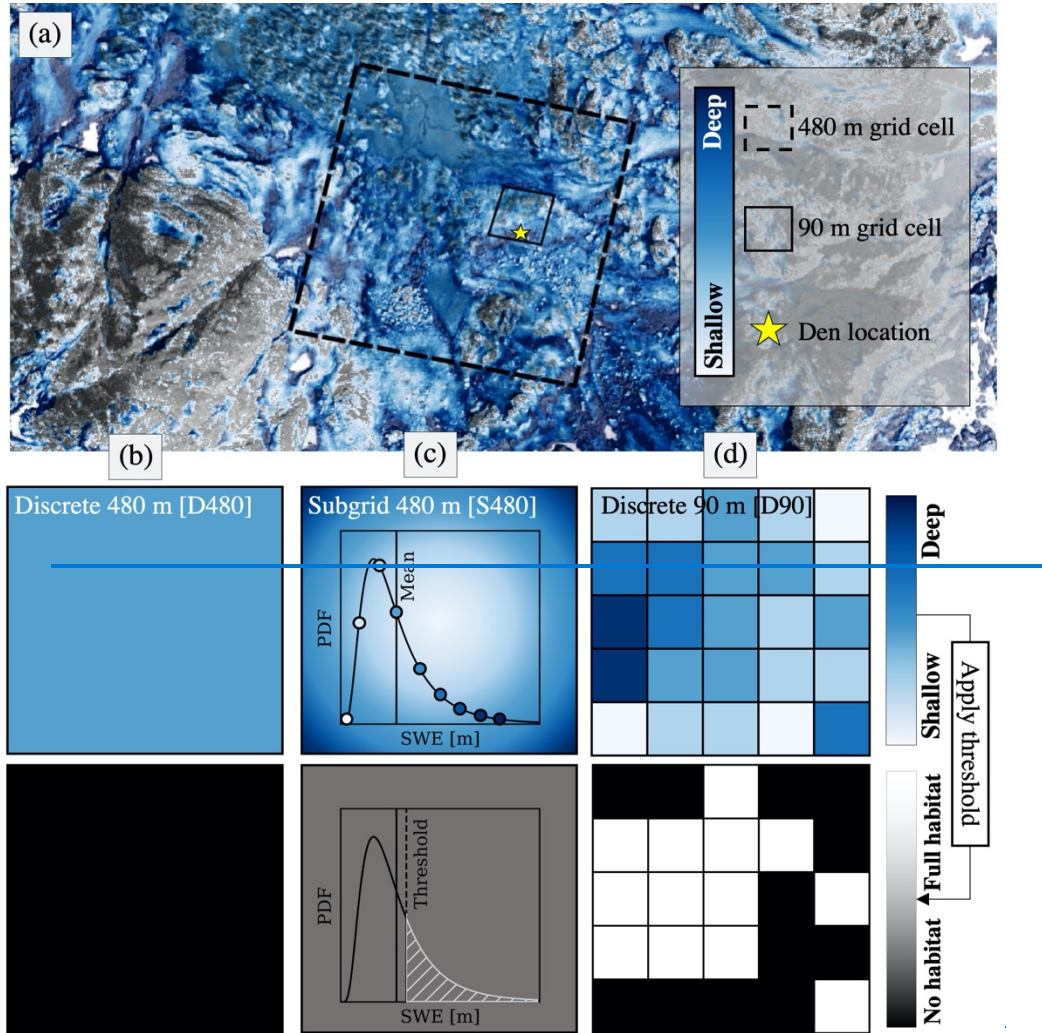
50 sensed observations (Dozier, 1989; Hall and Riggs, 2007; Sankey et al., 2015), partition snow accumulation and
51 snowmelt seasons (Cayan, 1996; Hamlet et al., 2005; Mote et al., 2005; Serreze et al., 1999), and parameterize
52 modeled processes like snow-layer formation and merging (e.g., Clark et al., 2015; Liston and Elder, 2006;
53 Wigmosta et al., 2002), rain and snow precipitation partitions (Auer, 1974; Harder and Pomeroy, 2013), and snow
54 holding capacity on steep slopes (Bernhardt and Schulz, 2010). Thresholds are also used to identify drought
55 conditions in snow-dominated watersheds (Dierauer et al., 2019; Harpold et al., 2017; Heldmyer et al., 2023)
56 (Dierauer et al., 2019; Harpold et al., 2017; Heldmyer et al., *In Review*), and the associated “decision trigger” and
57 “tipping point” thresholds that determine water use and allocation in regulated basins (Herman and Giuliani, 2018;
58 Kwadijk et al., 2010; Shih and ReVelle, 1995). However, despite widespread use, thresholds are often developed for
59 specific applications, and over short time intervals, decreasing the likelihood that a threshold developed for one
60 purpose could be applied in an identical manner to different periods of time, or to environmental products with
61 different characteristics (Härer et al., 2018; Jennings et al., 2018; Maher et al., 2012; Pflug et al., 2019).

62 Here, we focus on snow thresholds that have been used increasingly over the past decade to identify regions with
63 conditions suitable for the survival of snow-adapted wildlife. Many studies use thresholds that focus on snow
64 characteristics like snow depth, snow cover, snow density, snow water equivalent (SWE), and snowmelt season
65 snow persistence, which can be important for denning, migration, and food-availability for species like North
66 American wolverines (*Gulo gulo luscus*), polar bears (*Ursus maritimus*), and Dall sheep (*Ovis dalli dalli*) (Barsugli
67 et al., 2020; Durner et al., 2013; Liston et al., 2016; Mahoney et al., 2018; McKelvey et al., 2011; Sivy et al., 2018).
68 However, relatively few studies simulate snow at spatial resolutions that correspond to the features that drive snow
69 habitat (e.g., Glass et al., 2021; Liston et al., 2016; Mahoney et al., 2018). For instance, wolverines rely on snow
70 drifts for maternal and natal denning. These drifts often form a lee of obstructions near the forest edge and in talus
71 fields (e.g., Fig. 1, star). Yet, few models simulate snow at den-scale spatial-resolutions (< 10 m), and represent the
72 physical processes that control the formation of dens, like wind-redistribution, preferential deposition, avalanching,
73 and microtopographic shading. This is particularly the case for species status assessments which often attempt to
74 quantify wildlife habitat at large regional extents where high-resolution snow simulations with complex physical
75 processes would be computationally prohibitive. Thresholds are therefore used to facilitate the relationship between
76 a coarser-resolution representation of snow, and the finer-scale feasibility of wildlife habitat. The validity of this
77 approach is debated (e.g., Araújo and Peterson, 2012; Barsugli et al., 2020; Boelman et al., 2019; Bokhorst et al.,
78 2016; Copeland et al., 2010; Magoun et al., 2017). For example, coarser-scale representations of snow may resolve
79 the larger-scale meteorological influences on habitat availability, but coarser-scale representations of snow likely
80 overlook the smaller-scale refugia that could continue to support habitat, even with future changes to climate.

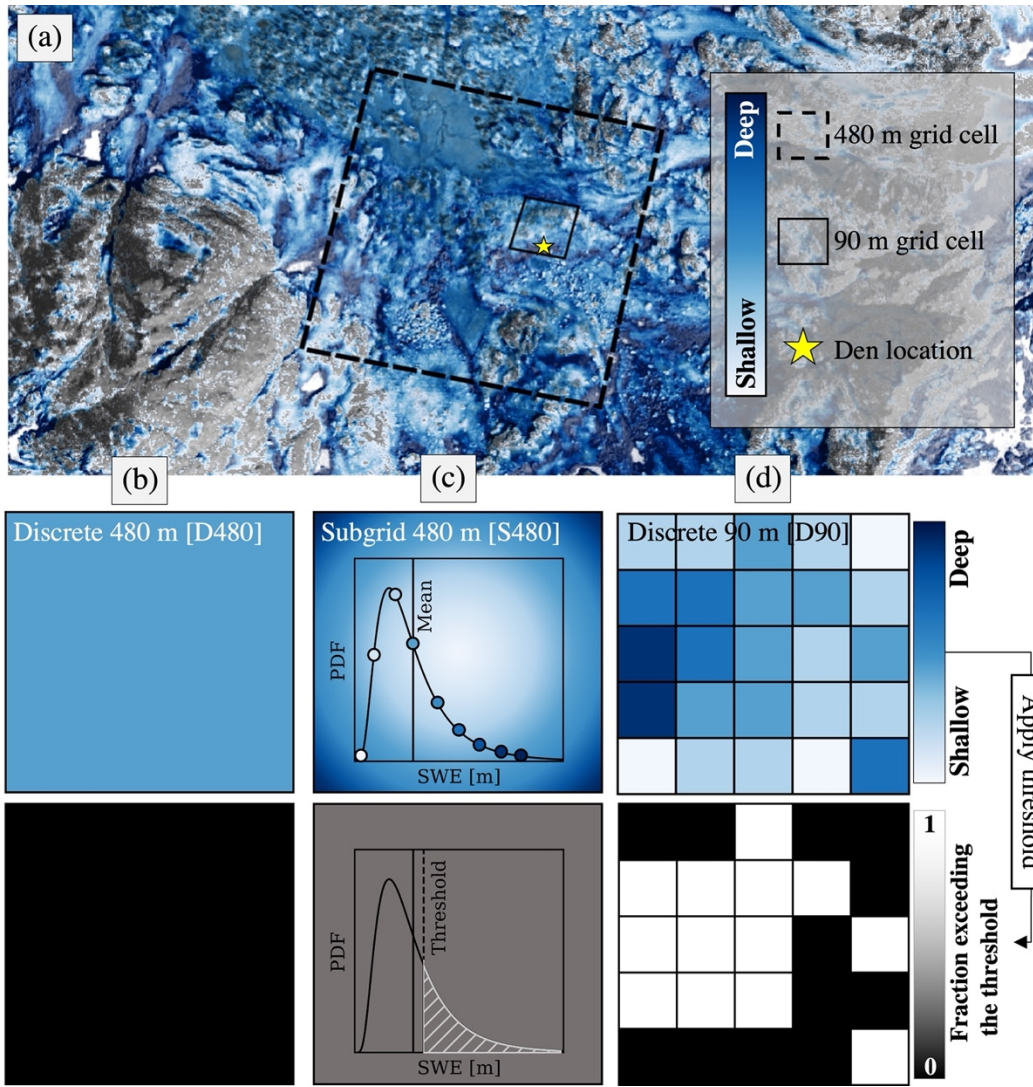
81 This manuscript study builds on work a study from Barsugli et al. (2020), which used physically-based simulations
82 to identify regions that could support wolverine denninghabitable areas using SWE thresholds, including a SWE
83 threshold (0.20 m) from known denning locations on a static date (15 May) corresponding to the tail end of the
84 maternal denning period (Copeland et al., 2010; McKelvey et al., 2011; USFWS, 2018) (Copeland et al., 2010; Heim
85 et al., 2017; McKelvey et al., 2011; USFWS, 2018). This 0.20 m SWE threshold was chosen based on 15 May SWE
86 that corresponded to known wolverine denning sites from a 250 m snow simulation (Barsugli et al., 2020; Ray et al.,
87 2017; USFWS, 2018). Barsugli et al. (2020) found that, relative to previous studies that used ~10 km products
88 (Laliberte and Ripple, 2004; McKelvey et al., 2011), snow simulations at 250 m resolution were able to better
89 resolve SWE persistence, and increased habitat, on shaded north-facing slopes. 250 m simulations also increased the
90 overall prevalence of snow that could support wWolverine denshabitat, both in current and future climates, over
91 Colorado and Montana Rocky Mountain domains.

92 Here, we extend the findings from Barsugli et al. (2020), testing the difference in wolverine denning supporthabitat
93 defined using thresholds (0.20 m SWE on 15 May) and a historic snow reanalysis with different spatial
94 discretizations (Fig. 1). These discretizations include: 1) discrete 480 m grid cells (D480), 2) discrete 90 m grid cells
95 (D90), and 3) 480 m grid cells with implicit representations of subgrid SWE spatial heterogeneity (S480). These
96 discretizations straddle the 250 m resolution used by Barsugli et al. (2020) and include both discrete (D480 and
97 D90) and implicit (S480) representations of snow distribution. These reanalyses, which combine snow modeling and
98 remotely-sensed observations of snow cover (more in Sect. 2.2), also resolve snow volume and distribution in
99 mountain terrain significantly better than more common modeling approaches (Pflug et al., 2022; Yang et al.,
100 2021) (Pflug et al., In Review ; Yang et al., 2021). We focus onover the same Colorado Rocky Mountain domain used
101 by Barsugli et al. (2020) over a longer period of 36 years, spanning 1985 to 2020. We address the following research
102 questions: 1) how does the spatial discretization of snow influence estimates of potential wolverine
103 denninghabitable area (PWDA)? and 2) is the sensitivity of PWDAhabitat to different snow spatial

104 discretizations greater or smaller than habitat sensitivity to interannual changes in winter climatic
 105 conditions? We also identify the spatial locations and causes of the greatest differences PWDA in thresholded
 106 wolverine habitat, and evaluate sensitivities to small uncertainties in both SWE thresholds (± 0.07 m) and threshold
 107 dates (± 2 weeks). More generally, this study highlights shortcomings, opportunities, and tradeoffs to thresholding
 108 spatial snow products, and serves as a roadmap for future wildlife habitat assessments.



109



110

111 Figure 1. SWE spatial heterogeneity inferred from airborne lidar at 1 m resolution, compared to 480 and 90 m grid
 112 cells, and a point (star) with a snow drift suitably deep for wolverine denning (a). SWE is simulated in this study
 113 using three different spatial discretizations: 480 m discrete grid cells (D480, column b), 480 m grid cells with
 114 subgrid SWE heterogeneity (S480, column c), and 90 m discrete grid cells (D90, column d). ~~Wolverine habitat~~
 115 ~~(bottom row) is defined for e~~ The fraction of the area that could support wolverine denning is estimated for each
 116 discretization on 15 May using a 0.20 m SWE threshold on 15 May. The fraction of the area exceeding the SWE
 117 threshold is binary (fully greater than or less than the threshold) ~~resholded habitat~~ for discrete grid cells (b and d) are
 118 binary (no habitat or full habitat), while the area exceeding the SWE threshold for habitat for the S480 subgrid
 119 discretization (c) is defined by the fraction of the grid cell SWE distribution with SWE exceeding the threshold
 120 (white hatching)

121 2. Domain and Data

122 2.1. Domain

123 We focused this work over Rocky Mountain National Park in Colorado state (Fig. 2). This domain is home to
 124 several snow-adapted wildlife species, and has been included in wolverine habitat assessments (Barsugli et al., 2020;
 125 McKelvey et al., 2011; USFWS, 2018). Barsugli et al. (2020) estimated most of the terrain supportive of wolverine
 126 habitat in this region to be between 2700 and 3600 m of elevation. Although ~~few wolverines have been sighted here,~~
 127 ~~and this area does not currently support a reproductive population of wolverines,~~ this region is of potential interest

128 for [wolverine species](#) reintroduction. More information about wolverine habitat can be found in the U.S. Fish and
129 Wildlife Service species status assessment (USFWS, 2018).

130 The Rocky Mountain National Park domain contained several snow observations (Fig. 2). These observations
131 included 28 snow telemetry (SNOTEL) stations, deployed and managed by the National Resources and
132 Conservation Service. These stations use snow pillows to measure the weight of snowpack and resulting SWE. A
133 distributed lidar observation of snow depth in southernmost portion of the domain was also collected by the National
134 Center for Airborne Laser Mapping in May 2010. These observations were used to assess the accuracy of the SWE
135 reanalysis discussed in Sect. 2.2.

136 2.2. SWE Reanalyses

137 SWE was calculated over the Rocky Mountain domain (Figure 2) ~~from using~~ a [popular](#) satellite-era (water years
138 1985 – 2020) probabilistic snow reanalysis (Margulis et al., 2019, 2016, 2015) performed at 3 arcseconds (~90 m)
139 and 16 arcseconds (~480 m). This reanalysis was generated at each individual grid cell using an ensemble of
140 simulations forced by the Modern-Era Retrospective analysis for Research and Applications, Version 2 (MERRA-2;
141 Gelaro et al., 2017), and simulated using the simplified Simple Biosphere Model, Version 3 (Xue et al., 1991)
142 coupled with the Liston (2004) snow depletion curve. The forcing dataset was downscaled to the simulation grid
143 (Giroto et al., 2014; Margulis et al., 2015) before running the land surface model. Model ensemble members were
144 provided different 1) precipitation multipliers (influencing total snow mass), 2) snow albedo decay functions
145 (influencing the rate of snow ablation), and 3) parameterizations of subgrid snow spatial variability (influencing
146 subgrid snow cover during snowmelt), among other parameters. The reanalysis then reweighted the ensemble
147 members to most-heavily favor those that matched the [snowmelt season evolution of fractional snow covered area
148 from 30 m Landsat observations. We expect uncertainties and errors in the snow reanalysis owing to both errors in
149 meteorological forcing data \(e.g., Daloz et al., 2020; Liu and Margulis, 2019\) and errors with the snow model \(e.g.,
150 Feng et al., 2008; Xiao et al., 2021\) satellite-observed snow cover disappearance throughout the snowmelt season.
151 However, the ensemble approach used by this reanalysis adjusted modeled snow accumulation and depletion to
152 track remote sensing observations of snow cover depletion, which has shown the capability to bias-correct SWE and
153 implicitly account for difficult-to-simulate processes like precipitation lapse rates, wind-loading/scour, avalanching,
154 and forest-snow processes \(e.g., Pflug et al., 2022; Yang et al., 2021\).](#)

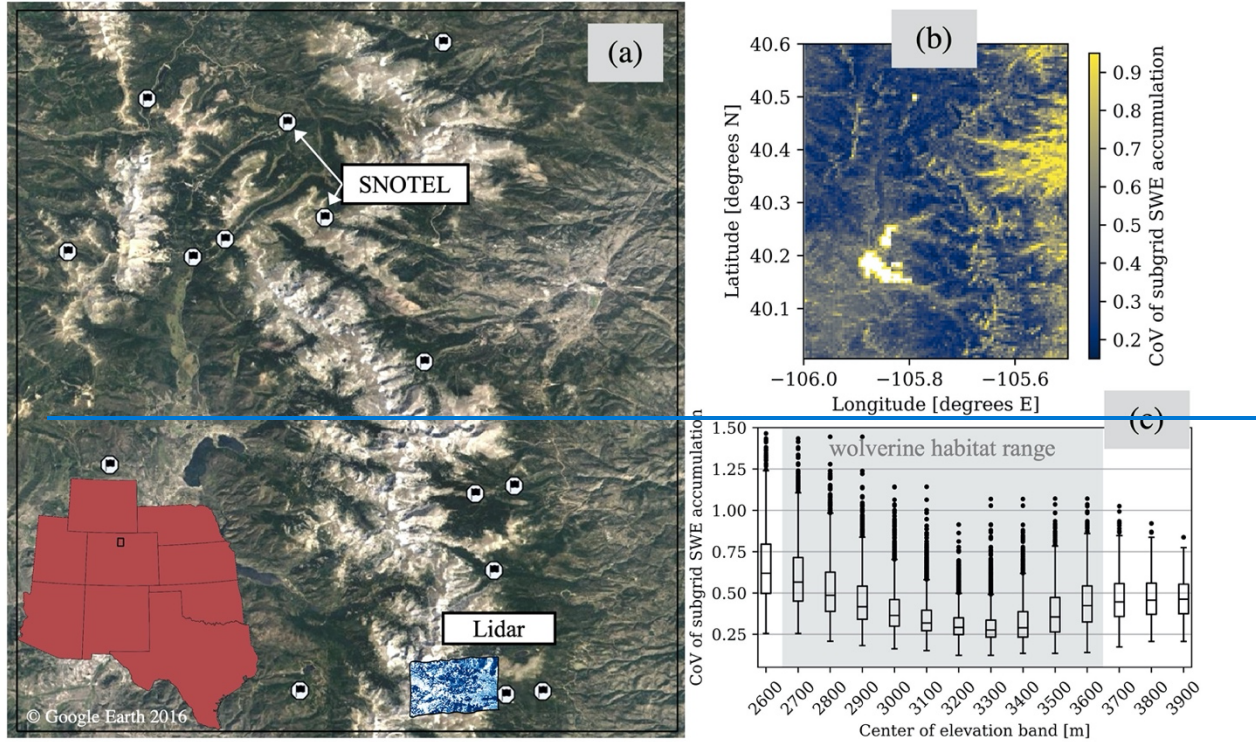
155 Relative to ~~independent~~ SNOTEL observations, ~~which are not used by the snow reanalysis, of SWE between 1985
156 and 2020 in the Rocky Mountain domain,~~ the reanalysis exhibited a [SWE](#) coefficient of correlation of 0.82 (~~not
157 pictured~~) [between 1985 and 2020 in the Rocky Mountain domain \(Fig. S1\)](#). On average, the reanalysis was biased
158 low relative to the snow pillow observations by approximately 23%. However, this could be attributed to the
159 location of SNOTEL observations in forested clearings (Fig. 2a) which typically have SWE deeper than the terrain
160 covered by the 480 and 90 m pixels (~~e.g., Livneh et al., 2014; Pflug et al., 2022~~) ([Livneh et al., 2014; Pflug et al., In
161 Review](#)). [While the snow reanalysis used in this study is ultimately a model product and subject to a number of
162 modeling uncertainties, the SWE simulated by the 90 m and 480 m discretizations agreed closely with each other
163 and with ground observations. Therefore, spatial differences in 15 May SWE, and the resulting distribution of snow
164 that exceeded the SWE threshold \(e.g., Fig. 1\) was attributable to differences in the interactions between the static
165 SWE threshold and different spatial discretizations of snow.](#)

166 For the 480 m grid cells with subgrid snow variability (Fig. 1c, S480), the heterogeneity of SWE was estimated
167 using a method developed by Liston (2004). This method assumes that the subgrid heterogeneity of SWE
168 accumulation is lognormally distributed, and is dictated by a time-constant coefficient of variation (CoV),

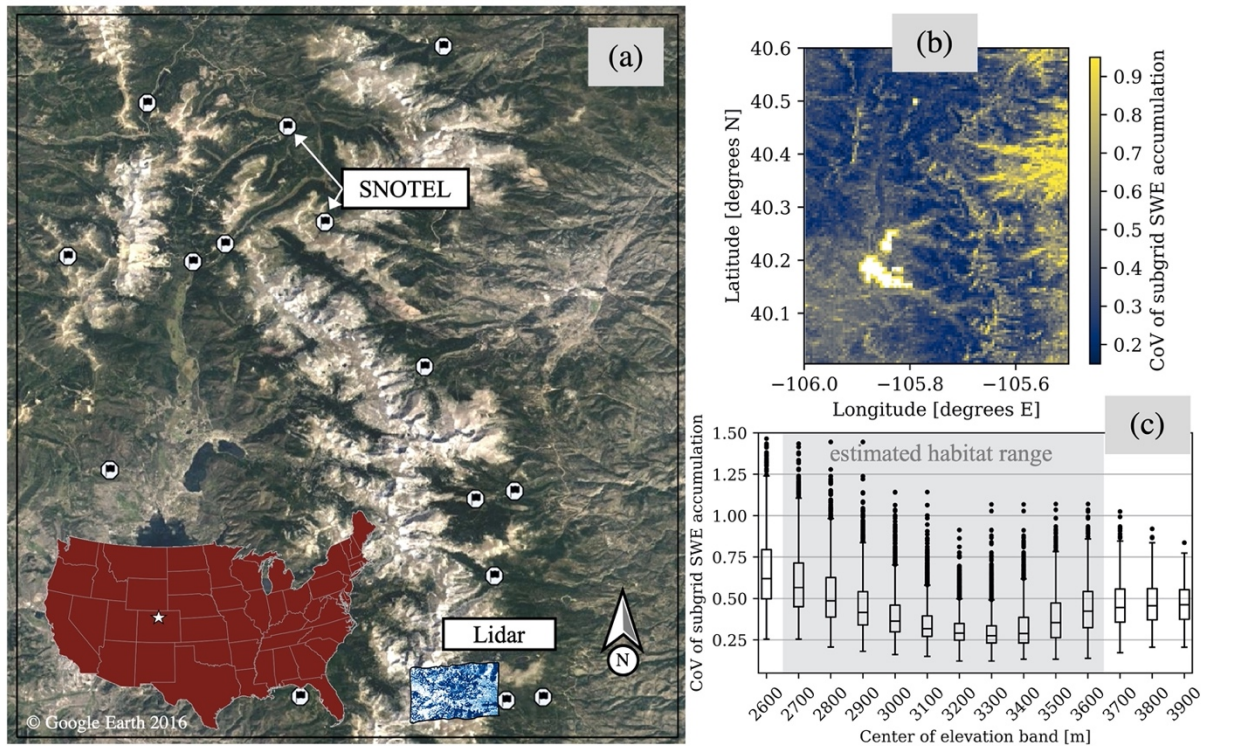
$$169 \quad \text{CoV} = \frac{\sigma}{\mu}, \quad (1)$$

171 where μ is the grid cell mean SWE and σ is the standard deviation of the SWE within that grid cell. The CoV of
172 subgrid SWE accumulation (Fig. 2b and 2c) was determined for each 480 m grid cell using the most common
173 pattern of SWE accumulation from the overlapping 90 m reanalysis grid cells (Fig. 1d) between 1985 and 2020
174 (detailed further in Text S1). In Sect. 3.1, we discuss how CoV was used to estimate the temporal evolution of
175 subgrid SWE heterogeneity.

176



177



178 Figure 2. Rocky Mountain National Park study domain. The location of SNOTEL observations and lidar snow depth
 179 observations are superimposed in the terrain map (a). The 480 m coefficient of variation of subgrid SWE
 180 accumulation is shown both spatially (b) and across 100 m elevation bands (c).

181 **3. Methods**

182 The methods evaluate the impacts of snow spatial discretizations and winter climatic conditions on assessments of
 183 total area suitable for [denning wolverines habitat](#). We investigated three different spatial discretizations; two
 184 discretizations using more common discrete representations of snow, and one with an implicit representation of
 185 subgrid snow heterogeneity (see Sect. 3.1). For each, [annual potential wolverine denninghabitable area](#)
 186 [\(PWDA\)\(WHA\)](#) was calculated using a static SWE threshold (0.20 m) on a static spring date (15 May) (Sect. 3.2).
 187 Finally, we partitioned years with winter precipitation magnitude and precipitation phase [climate categories \(wet,](#)
 188 [dry, cold, and warm\) anomalies, relative to average conditions from the snow reanalysis between water years 1985](#)
 189 [and 2020](#) (see Sect. 3.3). These [anomalies-categories](#) were used to examine whether winter climatic conditions or
 190 model representations of snow spatial distribution most-influenced estimates of [PWDAAnnual wolverine habitat](#).

191 3.1. Subgrid SWE evolution

192 The temporal evolution of subgrid SWE heterogeneity was estimated for 480 m grid cells (Fig. 1, S480) using
 193 methods developed by Liston (2004) (Fig. 3). Provided the reanalysis grid cell mean SWE (μ) from a [D480discrete](#)
 194 [480 m-grid cell \(Fig. 1b\)](#), and a CoV of subgrid SWE accumulation (Fig. 2b), the probability distribution of subgrid
 195 SWE for that grid cell ($f(SWE)$) was calculated using a lognormal distribution,

196

$$197 \quad f(SWE) = \left(\frac{1}{SWE\zeta\sqrt{2\pi}} \right) \exp \left[-\frac{1}{2} \left[\frac{\ln(SWE) - \lambda}{\zeta} \right]^2 \right],$$

198 (2)

$$199 \quad \lambda = \ln(\mu) - \frac{1}{2}\zeta^2,$$

200 (3)

$$201 \quad \zeta^2 = \ln(1 + CoV^2).$$

202 (4)

203 Figure 3b demonstrates the subgrid distribution of SWE in two winter periods (t_a^1 and t_a^2) assuming the mean SWE
 204 evolution from Fig. 3a, a CoV of 0.50, and Eq. 2 – 4.

205 In the snowmelt season, the Liston (2004) methodology assumes spatially-uniform snowmelt, causing snow
 206 disappearance first in locations with thinner SWE, and last in locations with deeper SWE. This can be
 207 conceptualized as taking the subgrid distribution of snow at peak SWE (Fig. 3b, t_2^a), and adjusting it downwards by
 208 a constant amount to reflect spatially-uniform melt (SWE_m) (Fig. 3c). In doing so, snow ~~would~~ only exists for
 209 portions of the gridcell where $f(SWE)$ at peak SWE was greater than SWE_m . Therefore, the fractional snow-
 210 covered area (fSCA) of the grid cell could be calculated from the fraction of the distribution ($f(SWE)$) with SWE
 211 greater than SWE_m ,

$$212 \quad fSCA = \int_{SWE_m}^{\infty} f(SWE)dSWE.$$

213 (5)

214 Since SWE_m can exceed the amount of SWE that exists in some locations at peak SWE timing, and since SWE
 215 cannot be less than 0 m (snow-absent), the change in gridcell mean SWE (μ) throughout snowmelt will not
 216 necessarily equal SWE_m . Rather, μ throughout the snowmelt season can be calculated from the expected value of
 217 the melt-shifted distribution (Fig. 3c),

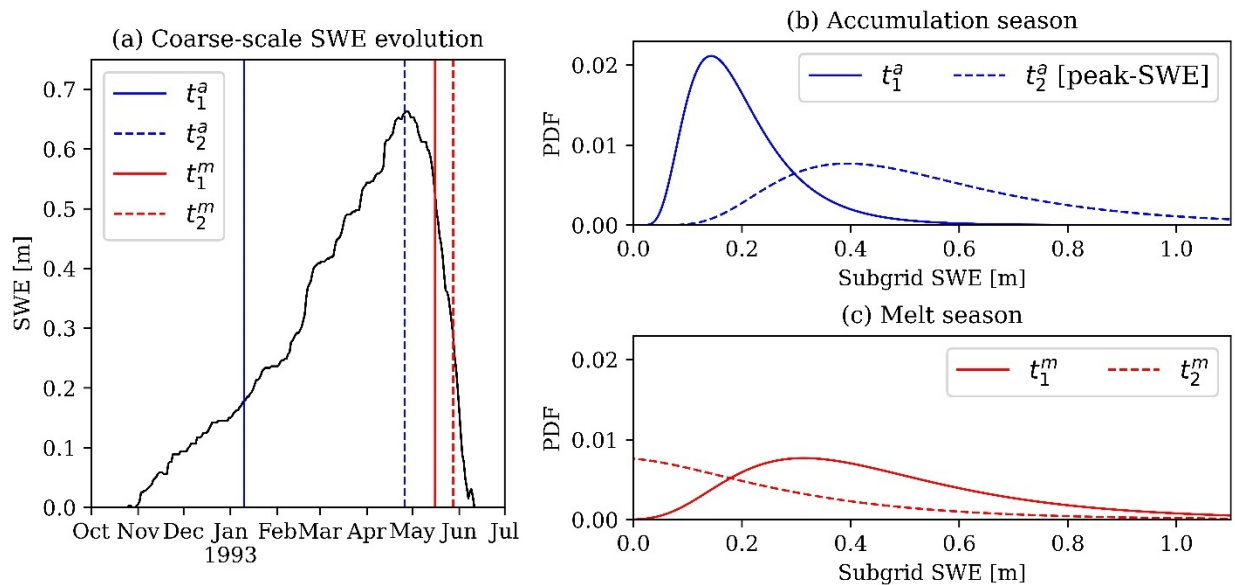
$$218 \quad \mu = \int_{SWE_m}^{\infty} [SWE - SWE_m]f(SWE)dSWE.$$

219 (6)

220 In this study, we were provided μ from the reanalysis at each 480 m grid cell and daily timestep. Using the CoV
 221 [calculated from the overlapping D90 data](#) (Fig. 2b), and maximum annual μ at each grid cell, we calculated the
 222 SWE distribution (Eq. 2) for each grid cell at peak SWE timing. Then, using a Newton-Raphson solver, we solved

223 the SWE_m for each grid cell that caused μ from Eq. 6 to match D480 μ from the 480-m reanalysis at each grid cell on
 224 15 May.

225 The Liston (2004) subgrid SWE parameterization discussed above operates under several assumptions. Like many
 226 other studies (e.g., Donald et al., 1995; Helbig et al., 2021; Jonas et al., 2009), Eq. 2 assumes that the distribution of
 227 snow accumulation at scales finer than the grid cell resolution can be represented by a lognormal distribution. We
 228 tested this assumption by evaluating the distribution of 1 m lidar snow depth observations (Fig. 2a) that fell within
 229 480 m grid cells. The Kolmogorov-Smirnov (KS) statistic, or maximum difference between cumulative distribution
 230 functions, was used to test how well different theoretical distributions (e.g., normal, lognormal, gamma, Rayleigh, chi,
 231 etc.) used by a variety of snow studies (e.g., He et al., 2019; Helbig et al., 2015; Mendoza et al., 2020; Pflug and
 232 Lundquist, 2020; Skaugen and Melvold, 2019) matched the lidar-observed snow depth distributions. The KS statistic
 233 for the lognormal distribution (Eq. 2) was 0.12 ± 0.05 , and was significantly worse (greater than 0.22) when
 234 comparing the observed lidar distributions versus other common distributions, like normal and gamma distributions.
 235 While not perfect, these results showed that subgrid snow heterogeneity was approximated best by lognormal
 236 distributions. The Liston (2004) subgrid methodology also assumed that the CoV of subgrid SWE accumulation was
 237 constant, resulting in a linear increase in SWE variability (standard deviation) with mean SWE throughout the snow
 238 accumulation season (Fig. 3b). While we lacked validation data to test this, this assumption is the basis for other
 239 modeling approaches, which scale snow input using information from historic snow accumulation patterns (Liston,
 240 2004; Luce et al., 1998; Pflug et al., 2021; Vögeli et al., 2016). Finally, although subgrid snowmelt is not spatially-
 241 uniform, melt-season snow heterogeneity is often modeled well by assuming uniform snowmelt. This is due to the
 242 outsized influence of snow accumulation spatial heterogeneity on snowmelt onset timing and snowmelt rates (Egli et
 243 al., 2012; Luce et al., 1998; Lundquist and Dettinger, 2005; Pflug and Lundquist, 2020). Here, we acknowledge that
 244 this approach operates on multiple assumptions (discussed above), all of which could vary in accuracy on grid cell
 245 level. However, this approach may also provide the opportunity to implicitly represent the heterogeneity of snow in
 246 complex terrain and the fraction of the area that could be more supportive for denning habitat (e.g., Fig. 1). We discuss
 247 this more in Section 3.2. Readers should refer to Liston (2004) for more information about the subgrid snow
 248 methodology described in this section.



249
 250 Figure 3. An example of the Liston (2004) subgrid SWE parameterization assuming $CoV = 0.5$, and SWE evolution
 251 for a 480 m grid cell in a random year (panel a). Subgrid SWE distributions are shown for two times (t , subscripts 1
 252 and 2) in the accumulation (superscript a) and melt (superscript m) seasons (panels b and c, respectively). The
 253 timing of each date corresponds to the matching vertical bar in panel a.

254 3.2. Thresholding wolverine habitable area

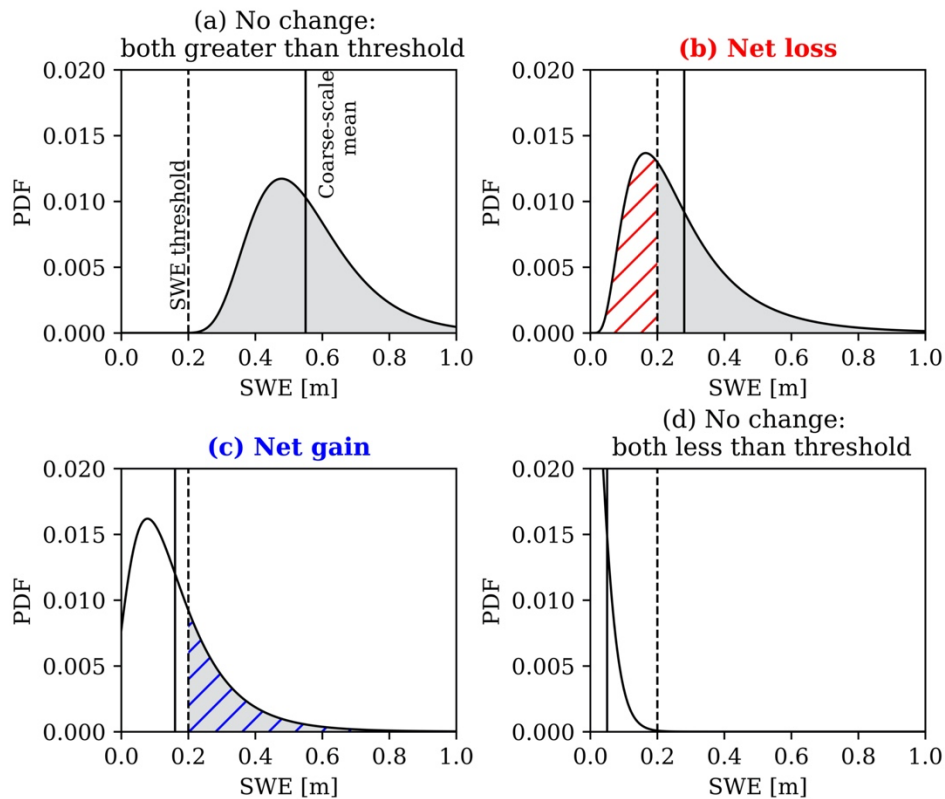
255 The area that could support denning wolverines habitat was calculated for each of the discretizations in each year
 256 using a SWE threshold of 0.20 m on 15 May, in accordance with previous studies (e.g., Barsugli et al., 2020;
 257 Copeland et al., 2010; McKelvey et al., 2011). For the 480 and 90-m discrete reanalyses (D480 and D90

258 discretizations), each cell's denninghabitable fraction (DHF) was classified as fully-suitable for denninghabitable
 259 (DHF = 1.0) or unsuitable/inhabitable (DHF = 0.0) if the 15 May grid cell-mean SWE was greater than or less than
 260 0.20 m, respectively. For the 480-m simulation with subgrid snow heterogeneity (S480 discretization), DHF was
 261 calculated for each grid cell using:

$$262 \quad DHF = \int_{SWE_m + \beta\alpha}^{\infty} f(SWE) dSWE, \quad (57)$$

264 which represented the portion of the cell's SWE distribution greater than the SWE threshold ($\beta\alpha = 0.20$ m).
 265 PWDA-WHA was calculated for each discretization as the sum of DHF (in space), multiplied by grid cell area.

266 Relative to DHF calculated from a discrete 480 m grid cell (D480), DHF calculated over the same area from the
 267 finer-scale discretizations (S480 and D90) could have one of four possible relationships. First, the mean SWE of the
 268 D480 grid cell, and the finer-scale distribution of SWE (S480 and D90), could both be entirely greater than the 0.20
 269 SWE threshold. This results in a fully-habitable-suitable denning fraction area (DHF = 1.0) for all discretizations
 270 (Fig. 4a). DHF would also agree in regions where all discretizations have SWE below 0.20 m (Fig. 4d), resulting in
 271 no denning opportunitieshabitat (DHF = 0.0). The scenarios shown in Fig. 4b and Fig. 4c are where DHF is sensitive
 272 to the discretization. Figure 4b shows a scenario where the coarse-scale-D480 mean SWE is sufficiently deep
 273 enough to be classified as fully-habitable-suitable for denning (SWE > 0.20 m), even though some portion of that
 274 grid cell contains SWE that is shallower than the SWE threshold. Therefore, using a finer-scale discretization would
 275 result in a net loss in DFhabitat relative to the D480 discretization, the magnitude of which is shown by the red
 276 hatching in Fig. 4b. Of course, the opposite could be true for instances where coarse-scale mean SWE falls
 277 below the 0.20 m SWE threshold, thereby underestimating denning opportunitieshabitat relative to finer-scale
 278 representations that resolve some deeper snow deposits (Fig. 4c, blue hatching). Here, Since the three reanalysis
 279 discretizations (D480, D90, and S480) we are provided identical meteorological forcing, and when coarsened to
 280 480m resolution, had resolve similar SWE that agreed to within 1%, on average on 15 May (within 1%). Therefore,
 281 the degree to which the scenarios shown in Fig. 4b and 4c occur were the drivers of habitat differences to wolverine
 282 denning opportunities.



284 Figure 4. Conceptual portrayal of the similarities (a and d) and differences (b and c) in ~~wolverine habitable~~
285 ~~fraction~~DF for a 480 m discrete grid cell (vertical solid line) and a finer-scale representation (distribution) of SWE
286 over the same area. The vertical dashed lines represent the 0.20 m SWE threshold. Shaded areas show the portion of
287 the distribution with SWE greater than the threshold. Hatched areas demonstrate differences in ~~DF~~habitat between
288 the coarser and finer-scale discretizations of SWE.

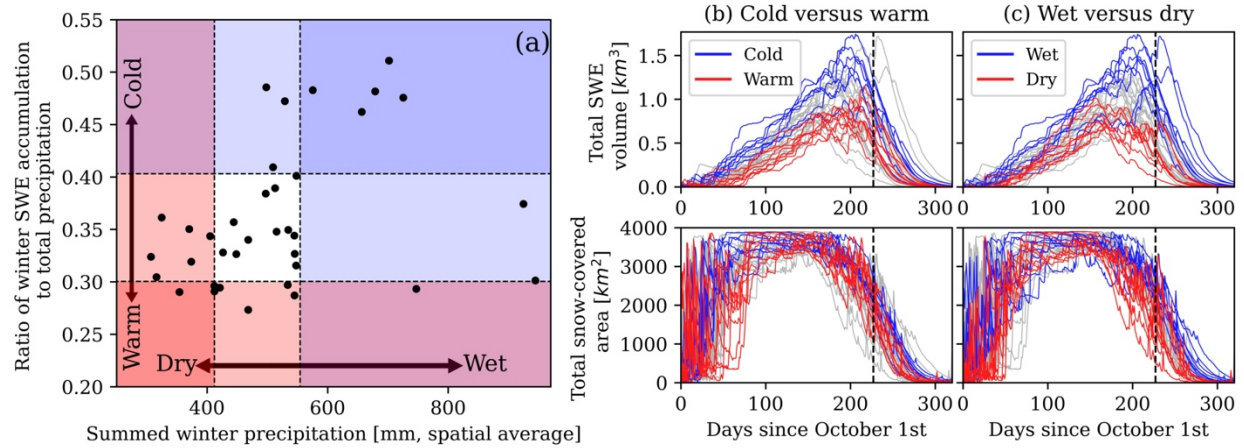
289 3.3. Categorizing winter climate ~~categories~~anomalies

290 To determine ~~PWDA~~WHA sensitivity to different climatic conditions, we identified years from the reanalysis with
291 ~~different~~anomalous winter precipitation magnitude and phase (rain versus snow). Here, winter is defined by periods
292 between October 1st and the date of domain peak SWE volume. Following work from ~~(Heldmyer et al., (2023),~~
293 ~~Heldmeyer et al. (in review),~~ we used ~~domain basin~~ average cumulative winter precipitation and the fraction of the
294 winter precipitation that fell as snow (both from the reanalysis) as indices for winter precipitation magnitude and the
295 temperature at which precipitation fell. Using a percentile, we separated years that fell at least that far from the 1985
296 – 2020 median precipitation magnitude and fraction of snow precipitation. In doing so, we partitioned years with
297 wet, dry, cold, and warm winter ~~climate categories~~anomalies. We did this separation using a range of percentiles
298 until the statistical difference (measured using the Mann-Whitney u-test) in D480 ~~PWDA~~WHA was maximized
299 between the years with different climatic conditions (warm, cold, wet, dry, and typical). To avoid spurious results,
300 this percentile was also adjusted to ensure that each ~~climate category~~anomaly included at least 6 years. This
301 approach maximized the difference in interannual ~~PWDA~~WHA as a function of different winter climatic conditions.
302 This was then used as the baseline to compare how much more or less sensitive ~~PWDA~~WHA was to the different
303 SWE spatial discretizations.

304 4. Results

305 ~~The spatial variability of subgrid SWE accumulation (Sect. 2.2 and Text S1) had a relationship with the terrain (Fig.~~
306 ~~2b and 2c).~~ Over low-elevation forested grid cells (< 2800 m), SWE accumulation variability was large relative to
307 the smaller amounts of snow, resulting in large CoV (typically between 0.50 and 0.80) (Fig. 2b and 2c). On mid-
308 elevation slopes (2800 – 3300 m), ~~where winter snowmelt was less common,~~ CoV tended to be smaller
309 (approximately 0.30, on average). However, CoV increased again at higher elevations (> 3300 m), and particularly
310 on the leeward side of peaks. This was expected given the more extreme terrain and increased spatial variability of
311 snow from wind-drifting, preferential deposition, cornice formation, and avalanching.

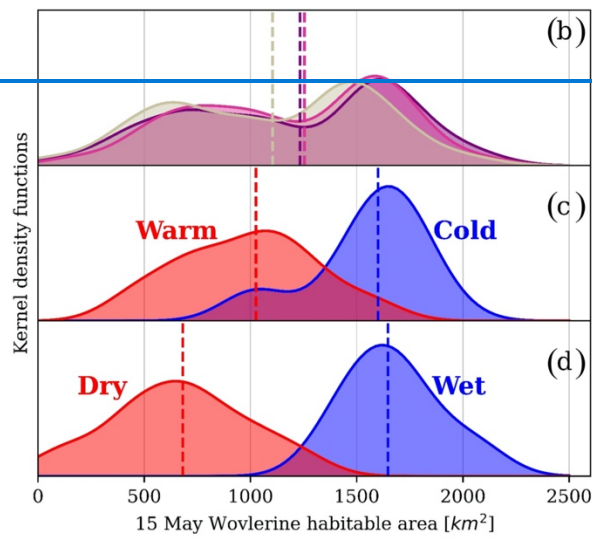
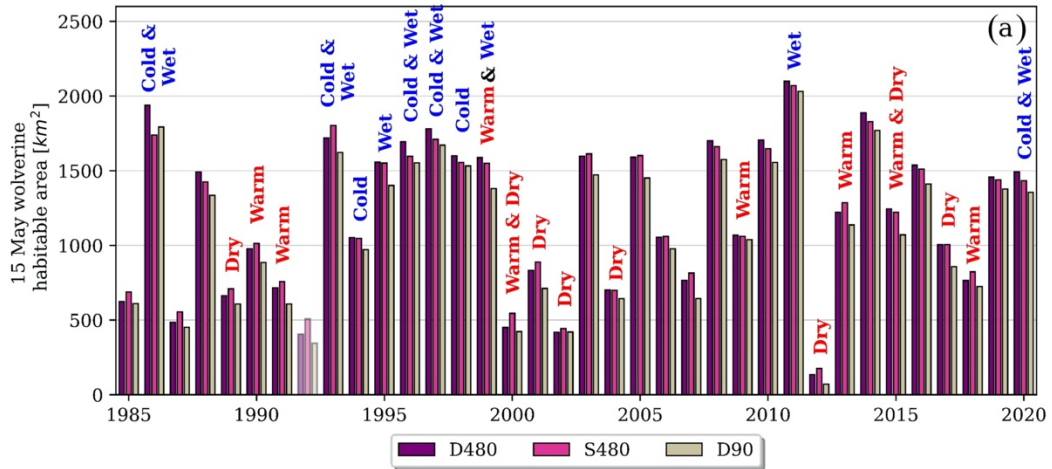
312 The difference in ~~PWDA-wolverine habitable area (WHA)~~ was maximized between 1) warm and cold years, and 2)
313 wet and dry years, that had winter precipitation magnitude (Fig. 5a, x-axis) and precipitation phase (Fig. 5a, y-axis)
314 that fell above the 77th and below the 23rd percentiles ($\pm 27^{\text{th}}$ percentile from the median). These ~~climate~~
315 ~~conditions~~anomalies had impacts on the ~~annual~~ evolution of SWE and snow-covered area (Fig. 5b and Fig. 5c). On
316 average, as compared to years with normal winter precipitation magnitude and phase (Fig. 5a, white region), cold
317 years and wet years had peak SWE volume that was 23% and 28% greater, respectively. This was opposed to warm
318 years and dry years, with peak SWE volume that was 21% and 31% smaller, on average, than typical water years.
319 The timing of peak-SWE was driven most by the magnitude of winter precipitation. In fact, average peak-SWE
320 timing was 28 days later for wet years than dry years. Snow disappearance timing (snow-covered area < 200 km²)
321 was also 21 days later for wet years than dry years. Statistically, the timing of snow disappearance, crucial for
322 wolverine denning habitat, was explained well by the peak-SWE volume ($r = 0.82$) and the date of peak-SWE ($r =$
323 0.63), both of which were influenced more by winter precipitation magnitude than temperature.

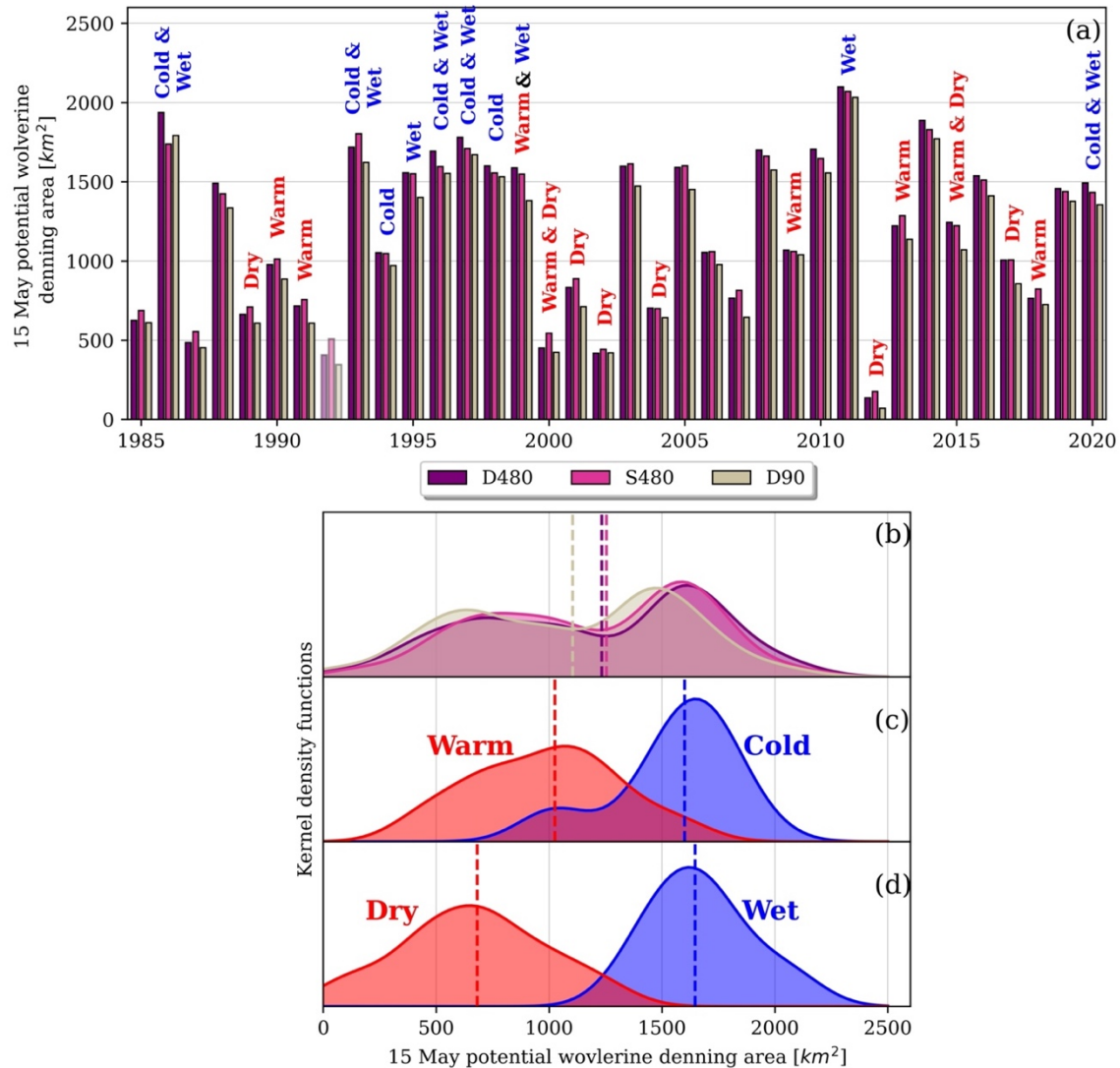


324

325 Figure 5. Annual climatic conditions grouped into ~~anomaly~~ categories based on winter precipitation magnitude (a,
 326 horizontal-axis) and precipitation phase (a, vertical-axis) outside the 23rd and 77th percentiles (a, dashed lines). The
 327 ~~annual~~ evolution of SWE volume and snow cover are compared for warm versus cold (column b) and wet versus dry
 328 years (column c). Vertical dashed lines in columns c and d indicate 15 May.

329 In all years except dry 2002, ~~PWDA_{WHA}~~ was smaller for the D90 discretization than the D480 discretization (Fig.
 330 6). This resulted in a 10% reduction to the 36-year median ~~PWDA_{WHA}~~ (Fig. 6b). The ~~PWDA_{WHA}~~ differences
 331 between the D480 and S480 discretizations varied more on an annual basis. For years with D480 ~~PWDA_{WHA}~~ less
 332 than 1000 km², S480 discretizations increased ~~PWDA_{WHA}~~ by up to 30%, 11% on average. However, in years with
 333 ~~PWDA_{WHA}~~ greater than 1000 km², S480 ~~PWDA_{WHA}~~ was approximately 3% smaller, on average, than D480
 334 ~~PWDA_{WHA}~~. In short, the S480 discretization tended to have ~~less dramatic~~ smaller annual swings in ~~PWDA_{WHA}~~
 335 than the D480 discretization. The causes of these ~~PWDA_{WHA}~~ disagreements are discussed in Sect. 5.1. Despite the
 336 ~~inter~~annual differences in D480 and S480 ~~PWDA_{WHA}~~, the 36-year median ~~PWDA_{WHA}~~ for these discretizations
 337 agreed to within 1% (Fig. 6b).





339

340 Figure 6. 15 May wolverine habitable area compared PWDA compared annually for three different spatial
 341 discretizations (a). Lower panels show the kernel distributions for the data in panel a, separated based on the spatial
 342 discretization (b), temperature anomalies-categories (c), and precipitation categories anomalies (d). The medians of
 343 each distribution are shown by the vertical dashed lines (b – d). The data in panels c and d include data from all
 344 three spatial discretizations. The data from WY1992 (a, faded bars) exhibited artifacts, and was excluded from the
 345 kernel distributions (b-d).

346 Even though PWDA-WHA was sensitive to different spatial discretizations (Fig. 6b), PWDA-WHA across the 36-
 347 year period was not statistically different between any of the three discretizations ($p > 0.48$). Conversely, the
 348 difference in 15 May PWDA-WHA was significantly larger between the years with different winter climate
 349 categories-anomalies (Fig. 6c and 6d). Differences in PWDA-WHA between years with anomalously warm and cold
 350 conditions were statistically significant ($p = 1 \times 10^{-5}$). Given that 15 May snow covered area were similar between
 351 warm and cold years (Fig. 5b), this difference between warm and cold years in Fig. 6c show that changes to PWDA
 352 were driven by changes to SWE magnitude and the area with SWE exceeding the SWE threshold, and Dry and wet
 353 years exhibited larger differences to both 15 May SWE and snow cover (Fig. 5c), resulting in PWDA (Fig. 6d) that
 354 was even more different between the years with dry and wet these climate conditions ($p = 1 \times 10^{-8}$). The impact of
 355 these warm, dry, cold, and wet climate conditions resulted in the bimodal distributions in PWDA shown for the
 356 different discretizations across the full time period (Fig. 6a). While PWDA-WHA was not statistically different
 357 between cold and wet years ($p = 0.34$), the distribution of PWDA-WHA in dry years was significantly smaller than

358 the distribution of PWDA_{WHA} in warm years ($p = 0.001$), showing that PWDA_{WHA} was more sensitive to
359 conditions that reduced snow habitat, like warm and dry conditions~~anomalies~~.

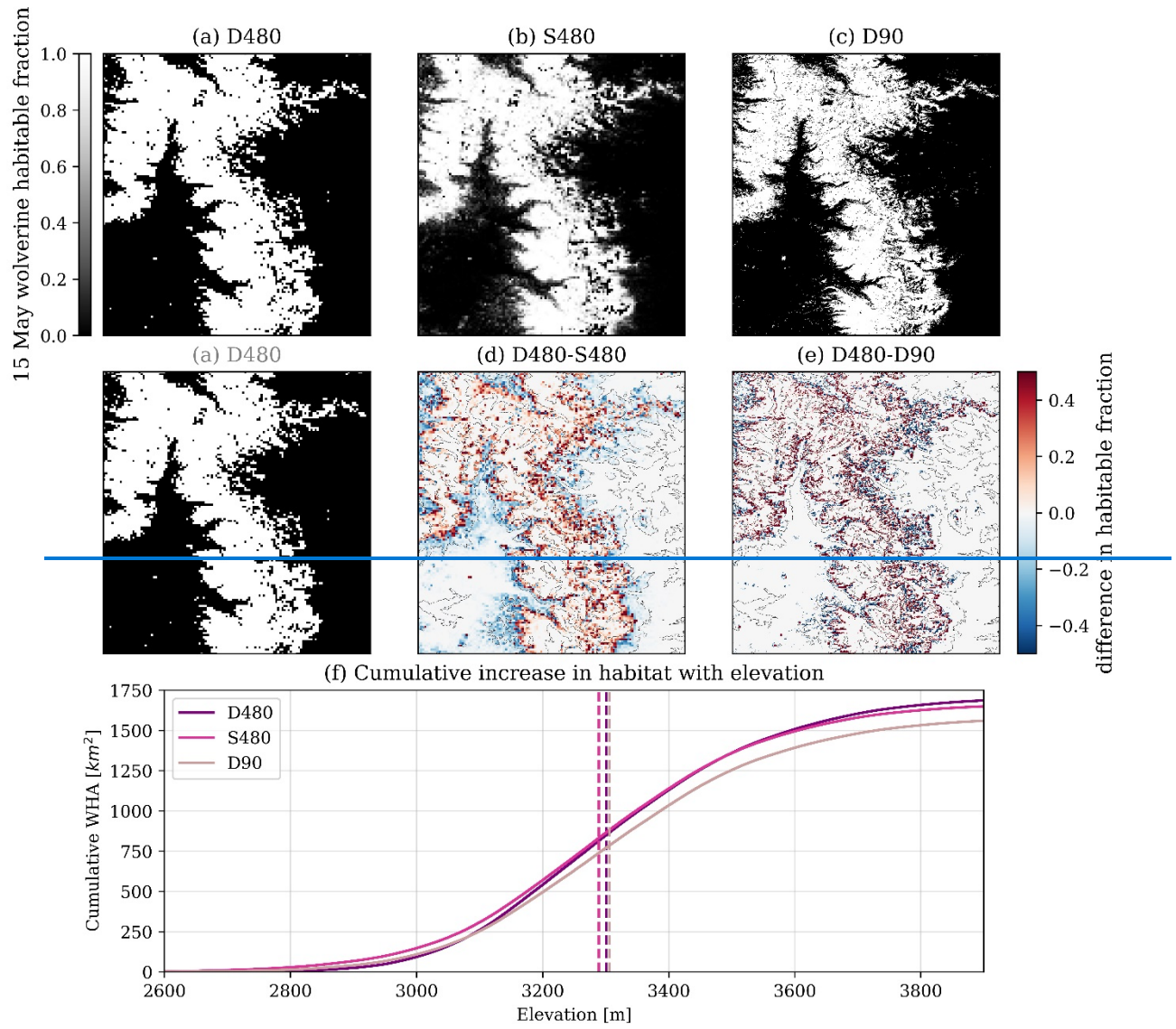
360 The results from Fig. 6 suggest~~ed~~ that changes in PWDA_{WHA} across annual periods of differing climatic
361 conditions, or across future periods with expected changes in climate (e.g., Barsugli et al., 2020) should be
362 informative from a species status assessment perspective, regardless of the snow spatial discretizations that we
363 tested here. However, as noted above, the S480 discretization increased PWDA_{WHA} by 11% on average in low
364 snow years, with increases as large as 30% for individual years. These low snow years often corresponded with drier
365 and/or warmer winter conditions, the latter of which are expected in the future. For example, the average air
366 temperature during December, January, and February precipitation events during warm years in the reanalysis
367 record was approximately 0.8° higher than winter precipitation events in typical years. These conditions are
368 consistent with what is projected for this region by 2055 (Eyring et al., 2016; Scott et al., 2016). This suggests that
369 the disparity between habitat inferred from discrete grid cells, and grid cells with subgrid snow heterogeneity, could
370 be of greater importance for future snow habitat assessments. Additionally, using PWDA_{WHA} as the sole metric for
371 evaluating differences in annual opportunities for wolverine denning~~habitat~~ may oversimplify the degree to which
372 static thresholds and different spatial discretizations interact. For instance, PWDA_{WHA} inferred on a static date (15
373 May) compares very different regimes of the snow season- as wet years had peak SWE timing, and snowmelt season
374 onset, that was 21 days later than typical snow seasons (Fig. 5). Since shallower snow melts more readily than
375 deeper snow (provided the same energy), comparing SWE_{WHA} on a static date in years with very different
376 conditions neglects the different rates of habitat depletion for a few days on either side of the date threshold. These
377 issues are investigated more in Sect. 5.

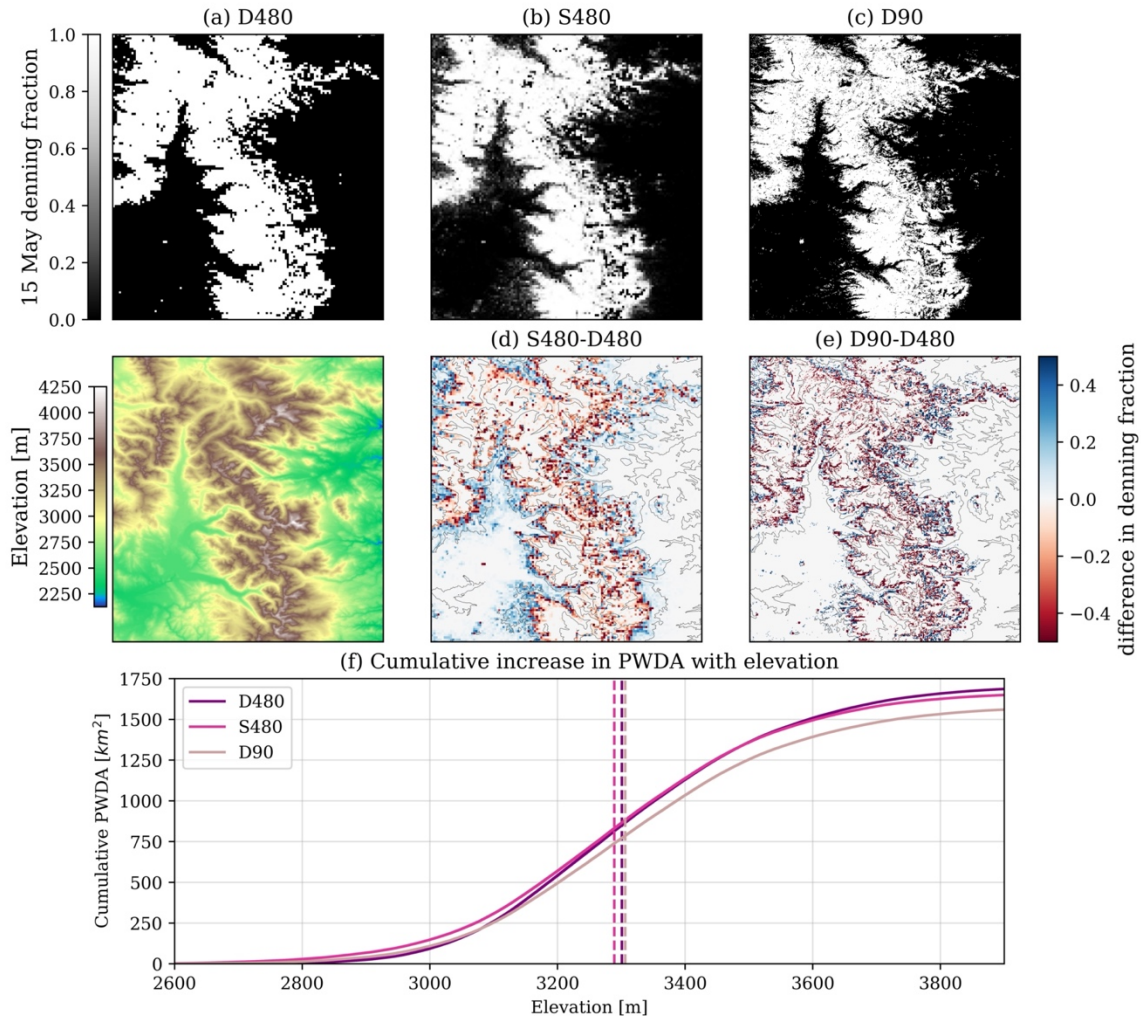
378 5. Discussion

379 In this section we diagnose the ~~locations and~~ causes for habitat disagreements in the frequency and locations at
380 which 15 May SWE exceeded the 0.20m SWE threshold between the three spatial discretizations of snow (Sect.
381 5.1). We also~~nd~~ investigate how the use of a static SWE threshold and threshold date, may obscure the picture of
382 interannual changes to snow-habitat~~wolverine denning habitat~~ availability (Sect. 5.2). Using these findings, we
383 discuss how information provided from multiple spatial discretizations could provide information about the fidelity
384 and uncertainty of thresholds, as well as the interactions and tradeoffs between spatial discretizations and thresholds,
385 both in context for assessing snow-adapted wildlife habitat, and more broadly for other environmental studies (Sect.
386 5.3).

387 5.1. Spatial-habitat differences in DF

388 The spatial difference in habitable fraction (HF)~~DF~~ between the three discretizations had annually similar patterns,
389 with the largest differences at locations where the domain had SWE that was near the 0.20 m SWE threshold. This
390 is was shown in~~illustrated in~~ Fig. 7d and Fig. 7c, where the greatest number of spatial DF disagreements that spiked
391 on 15 May 2008 were focused between approximately 2800 and 3200 m of elevation. Relative to the D480
392 discretization, the S480 discretization tended to increase DF habitat in grid cells at lower elevations where mean
393 SWE was less than the SWE threshold, but some portion of the grid cell had SWE deep enough to support
394 habitat~~exceed the threshold~~ (e.g., Fig. 4c). The opposite effect occurred at higher elevations where mean SWE
395 exceeded the SWE threshold, but the lower-tails of the S480 SWE distributions were below the threshold (e.g., Fig.
396 4b). As a result, the S480 discretization had a more-gradual increase in thresholded denning habitat~~availability~~ with
397 elevation, and a downward shift in the elevations that could support denning wolverines habitat (Fig. 7f). In fact,
398 relative to the D480 discretization, the S480 discretization had 23% less interannual variability in the elevation of
399 median habitat (Fig. S1a), or elevation at which equal PWDA_{WHA} existed at higher and lower elevations (Fig.
400 S2a). This was a result of the subgrid representations of SWE heterogeneity which allowed for gradual and
401 fractional ($0.0 \leq DF_{HF} \leq 1.0$) increases in DF_{HF} with increases in SWE. This was opposed to the D480
402 discretization, which could only resolve binary DF_{HF} (0 or 1 for SWE less than and greater than 0.20 m), resulting
403 in larger elevation~~topographical~~ shifts in the annual locations that could support wolverine denning~~of wolverine~~
404 habitat.





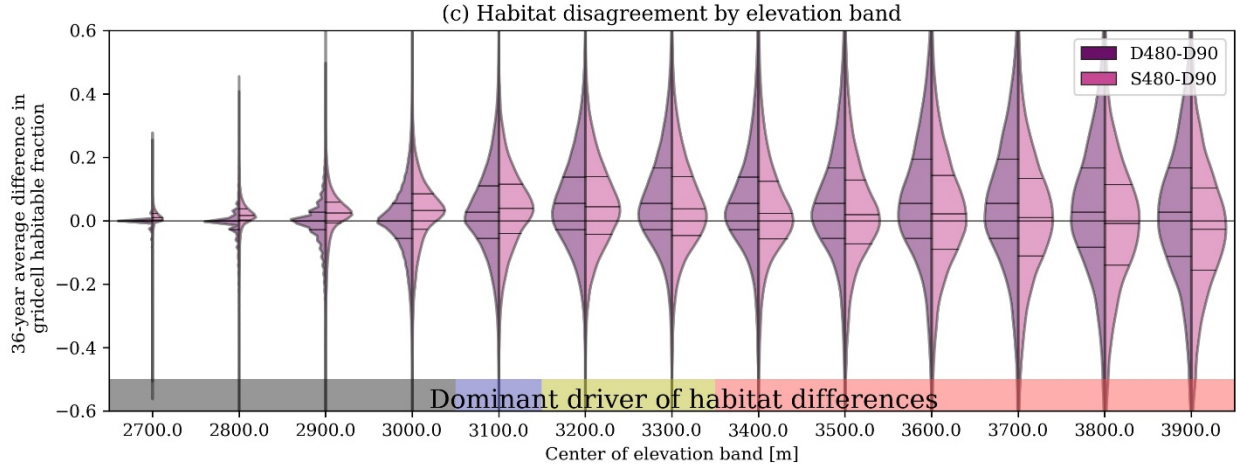
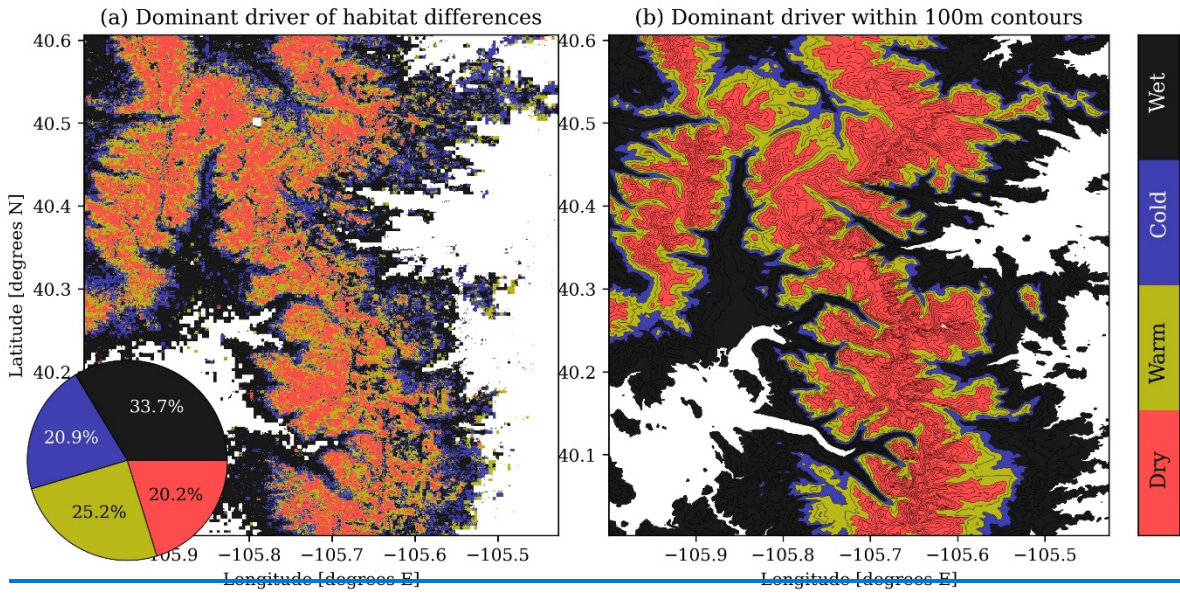
406

407 Figure 7. Spatial comparisons of [denning fractions](#) for the three discretizations on 15 May 2008. Panel f
 408 compares the cumulative [PWDA](#) (y-axis) calculated for grid cells sorted in order of increasing elevation (x-
 409 axis). Vertical dashed lines show the elevation of median [PWDA](#), or elevation at which [PWDA](#) is equal
 410 for higher and lower elevations.

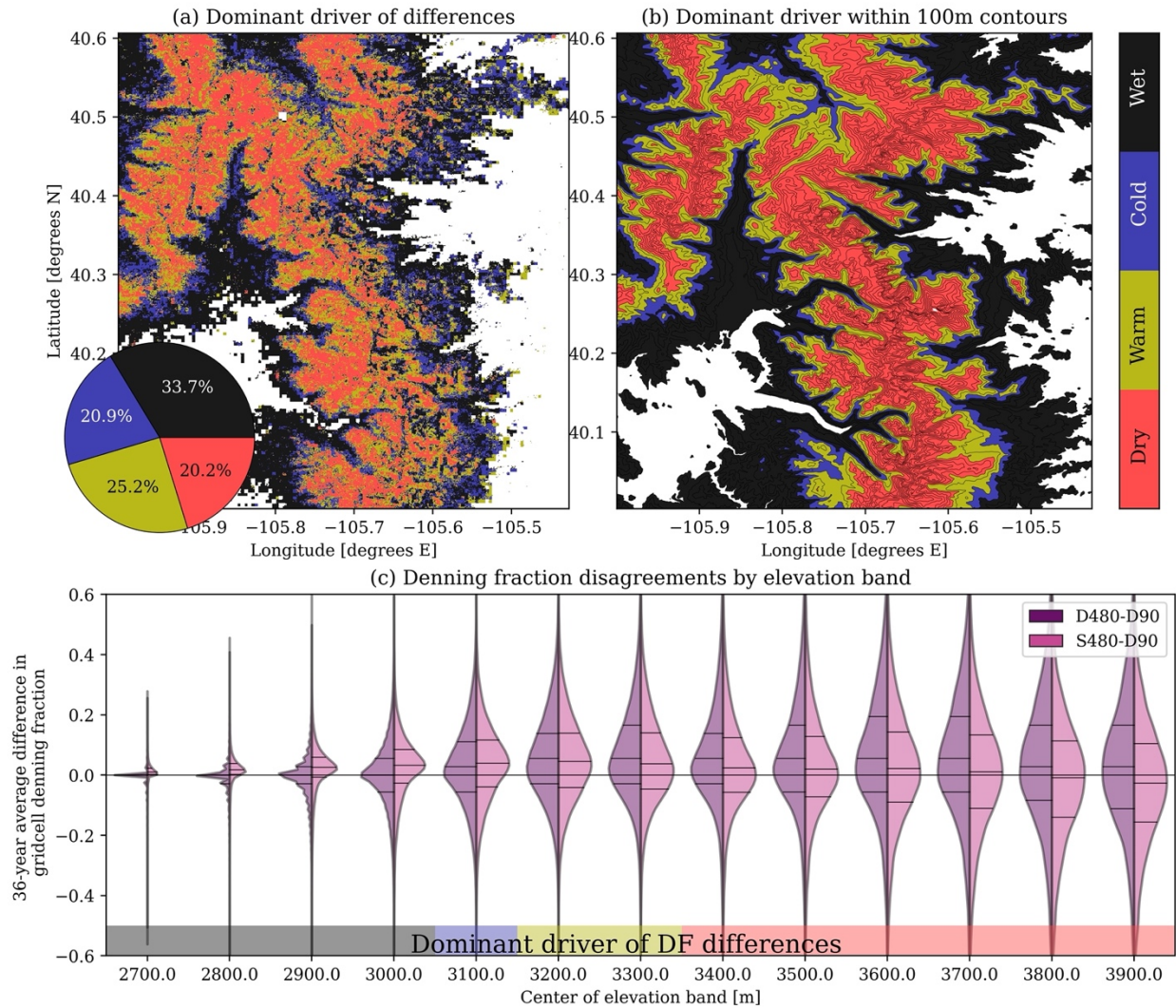
411 Relative to the D480 discretization, the D90 discretization also tended to increase [DF](#) at lower elevations.
 412 However, all years had reduced D90 [DF](#) in elevations higher than [the snow line approximately 3120m](#). This was
 413 the cause of the 10% reduction in D90 [PWDA](#), relative to the other discretizations (Fig. 6b). These decreases
 414 [in habitat](#) were typically located on unvegetated, exposed, and steep slopes, where it was likely that winter snow
 415 retention was decreased, snow sublimation was increased, and sloughing to lower-elevations was more common
 416 (Bernhardt and Schulz, 2010; Grunewald et al., 2014; Machguth et al., 2006). This demonstrates the utility of the
 417 observation-based reanalysis used in this study, which may have resolved thinner snow deposits on slopes with
 418 decreased snow retention and/or enhanced snow removal by processes like sloughing, both of which are among the
 419 most-difficult processes to represent with models. The D480 discretization averaged snow from surrounding areas,
 420 smoothing out thinner snow deposits resolved by the D90 discretization. Although attempting to resolve subgrid
 421 snow heterogeneity, the evolution of SWE assumed by the S480 simulation, which assumed lognormal snow
 422 accumulation and spatially-uniform subgrid snowmelt (Fig. 3), may have been less-appropriate for the areas
 423 containing these isolated thinner-snow 90 m grid cells. While the D90 discretization decreased total [PWDA](#),
 424 D90 snow cover was also patchier (Fig. 7c), which could also influence the movement and connectivity for
 425 [wolverines](#) (USFWS, 2018) and other snow-adapted species.

426 Winter precipitation magnitude and temperature influenced the volume of snow and the elevation of the snow line
427 that existed on 15 May in each year. Since the differences in DFHF between the discretizations were largest at grid
428 cells near the 0.20 m SWE threshold, often located just above the snow line, the spatial pattern of DFHF differences
429 (e.g., Fig. 7) exhibited an interannually-repeatable relationship with the dry, warm, cold, and wet winter climate
430 categories anomalies (Fig. 5). To show this, we calculated the differences in DFHF between all three discretizations
431 (D480 versus S480, D480 versus D90, and S480 versus D90) in all 36 years. Then, for each 480 m grid cell, we
432 calculated the climate anomaly that had the greatest absolute differences in HF. In other words, using the historic
433 36-year record, we identified/classified the meteorological condition/ climate category that resulted in the greatest
434 uncertainty-mean absolute differences in DFHF across the three discretizations for each 480-m grid cell. The climate
435 categories anomalies that had the greatest influence on DFHF uncertainties covered similar portions of the domain,
436 with 33.7%, 20.9%, 25.2%, and 20.2% being most attributed to dry, warm, cold, and wet conditions, respectively
437 (Fig. 8). At low elevations (2650 – 3050 m), 15 May snow typically existed only in wet years. In those years and
438 elevations, mean SWE for the D480 and D90 discretizations often fell below the 0.20 m SWE threshold. However,
439 the large CoVs of subgrid SWE accumulation in these elevations (Fig. 2) resulted in S480 subgrid SWE
440 distributions with upper-tails that sometimes/often exceeded 0.20 m (e.g., Fig. 4c), increasing total habitat (Fig. 8c).
441 This was in-line with findings from Magoun et al. (2017), who noted suitable denning conditions at lower-
442 elevations, even in instances when the surrounding terrain was predominantly snow-free.

443 The average differences in DFHF between the three discretizations were largest in cold years for elevations
444 spanning 3050 – 3150 m, and in warm years for elevations spanning 3150 – 3350 m (Fig. 8). Across this elevation
445 range (3050 – 3350 m), both of the 480 m discretizations (D480 and S480) estimated more denning
446 opportunities habitat than the D90 discretization (Fig. 8c). However, at higher elevations (> 3350 m), wolverine
447 habitat DF calculated from the S480 discretization inferred from the discretization with subgrid snow heterogeneity
448 (S480) approached DF calculated from the D90 thinner snow deposits estimated by the 90-m discretization (Fig.
449 8c).



450

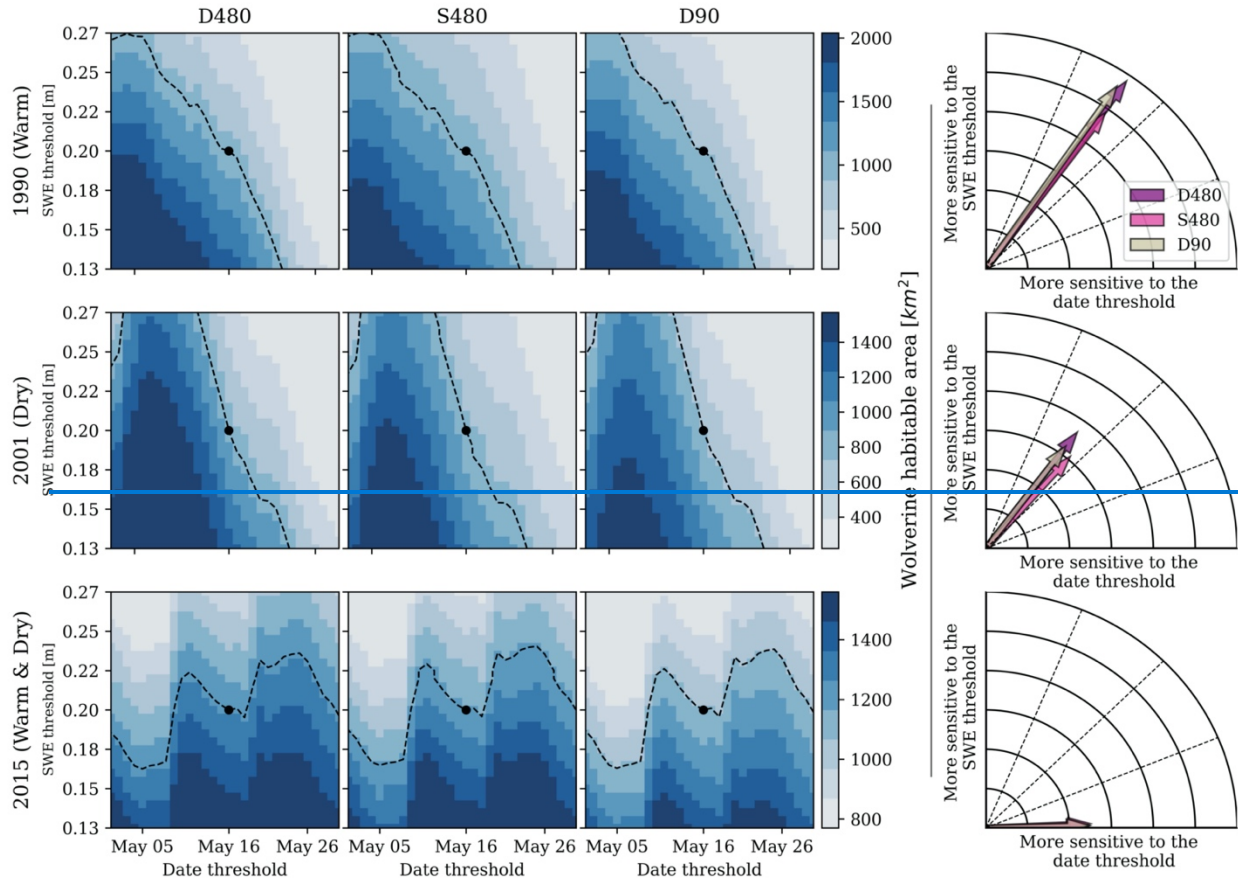


451
 452 Figure 8. Winter climate categories anomalies that most-influenced DFhabitat disagreements between the three
 453 discretizations (a). Panel b shows the most-prevalent common influence from panel a, for 100 m elevation bands.
 454 Using DFHF from the D90 discretization as a reference, the 36-year average difference in DFHF for the D480 and
 455 S480 simulations are shown by distributions for each 100 m elevation band (c). Lines inside the distributions show
 456 the median and interquartile range.

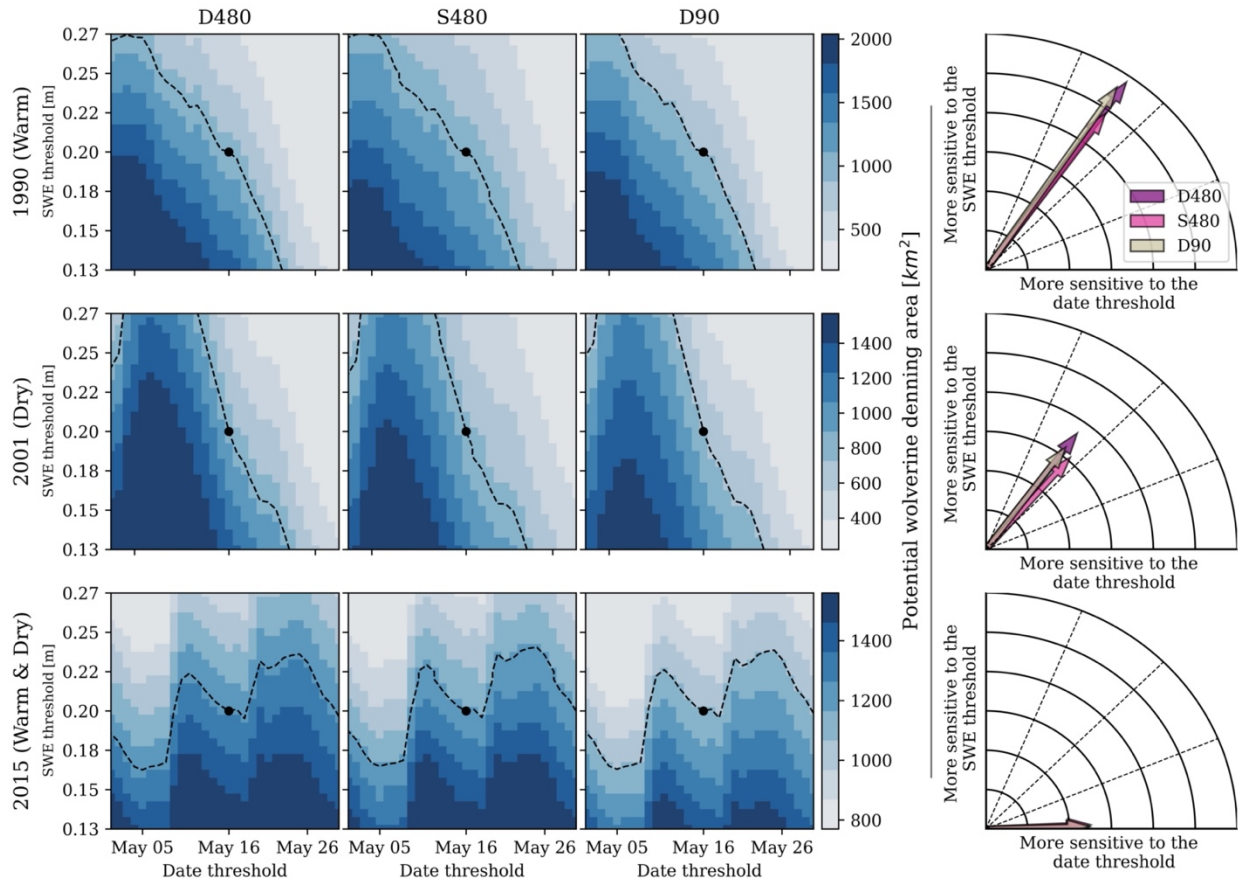
457 **5.2. Threshold sensitivities**

458 To this point, we assumed confidence in the SWE (0.20 m) and date (15 May) thresholds. However, small changes
 459 to either threshold could influence annual estimates of PWDAWHA (e.g., Copeland et al., 2010; Magoun et al.,
 460 2017). In Fig. 9, we show PWDAWHA calculated from a range of realistic SWE thresholds and threshold dates. The
 461 range of SWE thresholds (0.20 ± 0.07 m) were determined using a snow depth of 0.50 m, corresponding to
 462 observed wolverine dens (USFWS, 2018), and the 90th percentile range of 15 May snow densities from SNOTEL
 463 observations (Fig. 2a) between 1985 and 2020 ($260 - 540 \text{ kg/m}^3$). The range of threshold dates spanned a period of
 464 ± 2 weeks, corresponding to the difference in peak-SWE timing between dry and wet years (Fig. 5). This month-
 465 long time span is also consistent with the observed range of wolverine birth dates (Inman et al., 2012). This month-
 466 long time span also reflected the disparity between threshold dates and dates of observed wolverine habitat from
 467 multiple studies (Barsugli et al., 2020; Copeland et al., 2010; Magoun et al., 2017; McKelvey et al., 2011).
 468 PWDAWHA sensitivity was calculated using all combinations of SWE and date thresholds, both of which were
 469 discretized at 14 equally-spaced increments (Fig. 9, left). Then, the gradients (direction and magnitude of greatest
 470 change in PWDAWHA) were calculated from each unique combination of SWE and date thresholds. The gradients

471 were summed using vector addition (Fig. 9, right column) to determine 1) the total rate of change in PWDAWHA
 472 with changing thresholds (arrow length), and 2) the degree to which PWDAWHA was sensitive to one threshold
 473 versus the other (arrow angle). This process was repeated for each discretization and year.



474



475

476 Figure 9. PWDAWHA calculated using different SWE (y-axes) and date thresholds (x-axes), for the different
 477 discretizations (columns), in three different years (rows) with very different sensitivities. PWDAWHA calculated
 478 from the default thresholds (0.20 m SWE on 15 May) is shown by the black circle. Combinations of thresholds that
 479 could reproduce the default PWDAWHA are approximated by the dashed contour. The rightmost arrows show the
 480 total direction and magnitude of PWDAWHA changes with changes in the thresholds.

481 PWDAWHA in warm 1990 was 18% more-sensitive to the SWE thresholds than the threshold dates (Fig. 9, top
 482 row). To put this another way, the change in PWDAWHA across a period of ± 3 days from 15 May was
 483 approximately equal to the change in PWDAWHA from adjusting the SWE threshold by ± 2.5 centimeters. This
 484 sensitivity was similar to the average threshold sensitivity from the 36-year reanalysis record (Fig. S2+b). However,
 485 multiple years exhibited unique sensitivities. For example, spring snowfall between 1 May and 6 May 2001 (Fig. 9,
 486 middle row) caused PWDAWHA to both increase and decrease over the range of date thresholds (assuming a
 487 constant SWE threshold). Therefore, PWDAWHA changed based on whether the threshold date was before, during,
 488 or after the May snowfall event, buffering the degree to which thresholded denning habitat estimates were
 489 influenced by the specific winter meteorological conditions that occurred in that year. This effect also occurred in
 490 2015, when 15 May fell between two spring snowfall events (Fig. 9, bottom row). As a result, PWDAWHA tended
 491 to increase, on average, over the range of threshold dates, resulting in heightened sensitivities to the date on which
 492 denning opportunities habitat was evaluated. These spring snowfall events had large impacts on 15 May
 493 PWDA, but are unlikely to accurately represent the habitat opportunities and stresses that wolverine were subject to
 494 in that year. This demonstrates the dangers of thresholds applied on static dates, and suggest that metrics over
 495 multiple dates (e.g., number of May days exceeding a SWE threshold) and across sequences of years could be more
 496 accurate representations of snow refugia. Overall, WHA varied by as much 82% between the realistic thresholds
 497 shown in Fig. 9. This was similar in magnitude to the differences in WHA between years with opposing winter
 498 climate anomalies (Fig. 6c and 6d).

499 Overall, PWDAWHA varied by as much 82% between the realistic thresholds shown in Fig. 9. This was similar in
 500 magnitude to the differences in PWDAWHA between years with opposing winter climate anomalies (Fig. 6c and

6d). Across the years evaluated in this study, in most years, the sensitivities to the thresholds were largest for the D480 simulation, and smallest for the S480 simulation (Fig. 9 and Fig. S24b). As discussed in Sect. 5.1, the S480 discretization, which represented subgrid snow distribution and fractional changes to $\frac{DFHF}{SWE}$ with changes to the SWE threshold and threshold date, had less sensitivity to interannual changes in meteorological conditions. Similarly, small changes in the SWE threshold and threshold date changed the prevalence of snow habitat snow that exceeded the static threshold for discrete grid cells by larger amounts than the S480 discretization. This suggests that studies with subgrid representations of snow heterogeneity may decrease the overall sensitivity to SWE and date thresholds. ~~uncertainties.~~

5.3. Threshold caveats and future suggestions

The D90 and S480 discretizations provided unique, but different advantages for estimating $PWDA_{WHA}$. We believe that the upper-elevation decreases in D90 SWE and denning habitat on steep and unvegetated surfaces were realistic. These results were contrary to the findings from Barsugli et al. (2020), who in the same domain, found that finer-scale physically-based simulations resulted in net increases in wolverine denning opportunities habitat. However, this analysis used a joint model and observation-based approach (Sect. 2) that may have implicitly represented decreased snow retention and/or snow sloughing better than the physically based models used by Barsugli et al. (2020). The discretization with subgrid snow heterogeneity (S480), which is not as commonly used, had less-dramatic swings in total habitat $PWDA_{WHA}$ with changes in annual winter climatic conditions (Fig. 6) and thresholds (Fig. 9). We therefore think that subgrid representations of snow may be important for habitat assessments, especially given that snow deposits suitable for denning at scales of 10 m or less sometimes may occur in regions with otherwise little snow (Magoun et al., 2017).

The results of this study suggest that uncertainties provided from combinations of multiple discretizations, applied across a range of realistic thresholds, would be more informative than a single discretization and set of thresholds. For instance, SWE volume on 15 May 2015 was 10% less than the 36-year median 15 May SWE volume. However, due to spring snowfall (Fig. 9), SWE volume on 30 May 2015 was 31% greater than the 36-year median on the same date. ~~The static 15 May threshold date thereby failed to capture the boost to wolverine habitat provided by snowfall a few days after 15 May.~~ Multiple discretizations could also be used to identify the locations of most (e.g., Fig. 4a and 4d) and least-certain (Fig. 4b and 4c) opportunities for denning habitat. This information could be used as the basis for identifying the locations where remote sensing or field campaigns could hone annual estimates of refugium habitat, given that year's meteorological conditions. Altogether, differences across discretizations (e.g., Fig. 6) and threshold sensitivities (e.g., Fig. 9) could also be used to provide uncertainty bounds for $PWDA_{WHA}$ calculated in any given year.

Our results show that caution is warranted when combining gridded data and static thresholds. While we focus on the impact that thresholds and different snow spatial discretizations have on approximations of wolverine denning opportunities wolverine habitat, we expect these results to be applicable to other environmental applications. For instance, while temperature thresholds are widely used to partition rain and snow precipitation in models, temperature discretized at different spatial scales could influence the spatial variability of temperature and resulting snowfall volume thresholded across one or many snowfall events (e.g., Jennings et al., 2018; Nolin and Daly, 2006; Wayand et al., 2017). Snow cover thresholded using visible and infrared satellite observations may also require changes based on the size of the satellite pixels and the underlying topographic and vegetative characteristics (Härer et al., 2018; Pestana et al., 2019). Future studies should report the extent to which different spatial discretizations and ranges of realistic thresholds influence results. This information could be used to report the 1) uncertainty of thresholded outputs, 2) fidelity of different gridded products, and 3) the degree to which multiple spatial discretizations could be combined to improve the fidelity and transferability of results.

6. Conclusions

Potential wolverine denning habitable area ($PWDA_{WHA}$) was thresholded using a published SWE threshold (0.20 m) on a threshold date (15 May) in a Colorado Rocky Mountain domain between 1985 and 2020. Results showed that $PWDA_{WHA}$ was statistically different ($p < 0.01$) between years with different winter precipitation magnitude (wet versus dry) and precipitation temperature (cold versus warm) conditions anomalies. In fact, climate-driven differences in annual $PWDA_{WHA}$ were substantially larger than differences in $PWDA_{WHA}$ between snow discretized using 1) discrete 480 m grid cells, 2) 480 m grid cells with subgrid representations of SWE heterogeneity, and 3) discrete 90 m grid cells. Therefore, studies that assess changes in total habitat habitat health for species like wolverines with past and future changes in climate could be informative, regardless of the spatial discretizations tested.

554 Despite the sensitivity to winter climatic conditions, annual differences in spatial habitat denning patterns and
555 parameter sensitivities emerged for the different discretizations. For instance, 90 m grid cells resolved thinner snow
556 deposits in mid-to-upper elevations (approximately 3050 – 3350 m) that were not resolved by either of the 480 m
557 discretizations, decreasing PWDA-WHA by 10%, on average. Snow discretized with subgrid representations of
558 SWE spatial heterogeneity also had less-dramatic swings in annual PWDA-wolverine habitat. The simulations with
559 subgrid SWE heterogeneity increased snow-habitat-PWDA by 10 – 30% in low-snow years, many of which were
560 representative of future changes in average temperature expected over the next 50 years. Spatially, the differences in
561 wolverine habitat the prevalence of SWE that exceeded the threshold between the three different snow discretizations
562 were heightened at the grid cells that had SWE values close to the SWE threshold (0.20 m) on 15 May, the elevation
563 of which was driven in large part by the winter climatic conditions. On average, wolverine habitat-PWDA was -18%
564 more sensitive to the SWE threshold than the date threshold, but had the smallest amount of sensitivity to the 480 m
565 simulation with subgrid snow heterogeneity, which allowed-for-had more gradual changes to the fraction of a region
566 exceeding the SWE threshold-wolverine habitat with small changes in SWE. This discretization also had the least
567 amount of habitat-sensitivity to interannual changes in winter climatic conditions. However, some years had late-
568 spring snowfall events, altering the amount of wolverine habitat-PWDA by up to 82% depending on whether the
569 threshold date was before, during, or after the snowfall event.

570 Our results show that differences in how snow is spatially discretized can influence information generalized using
571 thresholds. Therefore, future studies thresholding spatiotemporal environmental data should include multiple spatial
572 discretizations and ranges of realistic thresholds to provide a more comprehensive picture of uncertainties associated
573 with chosen thresholds and datasets. Although we used wolverine habitat as an example, we expect these results to
574 be applicable to any study thresholding environmental data, especially for studies generalizing information at spatial
575 scales finer than those of modeled or observed resolutions.

576 **Code and data availability**

577 Readers are encouraged to enquire about the most up-to-date version of the reanalysis from the principal developer,
578 Steven Margulis. Scripts used in this manuscript are provided at [https://github.com/jupflug/HABITAT-](https://github.com/jupflug/HABITAT-threshold_vs_discretization)
579 threshold_vs_discretization.

580 **Author contributions**

581 JP and BL designed the experiments. YF and SM provided the snow reanalysis. JP wrote the manuscript, with
582 comments provided from all authors, and special supervision by BL.

583 **Competing interests**

584 The authors declare that they have no conflict of interest.

585 **Support**

586 This work was supported by the CIRES Visiting Fellows Program and the United States Geologic Survey (USGS)
587 award G21AC10645.

588 **Acknowledgements**

589 We would like to thank and acknowledge support from current and past U.S. Fish and Wildlife Service staff, in
590 particular, John Guinotte and Steve Torbit.

591 **References**

- 592 Araújo, M.B., Peterson, A.T., 2012. Uses and misuses of bioclimatic envelope modeling. *Ecology* 93, 1527–1539.
593 <https://doi.org/10.1890/11-1930.1>
- 594 Auer, A.H., 1974. The Rain versus Snow Threshold Temperatures. *Weatherwise* 27, 67–67.
595 <https://doi.org/10.1080/00431672.1974.9931684>
- 596 Barsugli, J.J., Ray, A.J., Livneh, B., Dewes, C.F., Heldmyer, A., Rangwala, I., Guinotte, J.M., Torbit, S., 2020.
597 Projections of Mountain Snowpack Loss for Wolverine Denning Elevations in the Rocky Mountains.
598 *Earths Future* 8, e2020EF001537. <https://doi.org/10.1029/2020EF001537>
- 599 Bernhardt, M., Schulz, K., 2010. SnowSlide: A simple routine for calculating gravitational snow transport. *Geophys.*
600 *Res. Lett.* 37. <https://doi.org/10.1029/2010GL043086>
- 601 Boelman, N.T., Liston, G.E., Gurarie, E., Meddens, A.J.H., Mahoney, P.J., Kirchner, P.B., Bohrer, G., Brinkman,
602 T.J., Cosgrove, C.L., Eitel, J.U.H., Hebblewhite, M., Kimball, J.S., LaPoint, S., Nolin, A.W., Pedersen,

603 S.H., Prugh, L.R., Reinking, A.K., Vierling, L.A., 2019. Integrating snow science and wildlife ecology in
604 Arctic-boreal North America. *Environ. Res. Lett.* 14, 010401. <https://doi.org/10.1088/1748-9326/aaec1>

605 Bokhorst, S., Pedersen, S.H., Brucker, L., Anisimov, O., Bjerke, J.W., Brown, R.D., Ehrich, D., Essery, R.L.H.,
606 Heilig, A., Ingvander, S., Johansson, C., Johansson, M., Jónsdóttir, I.S., Inga, N., Luoju, K., Macelloni,
607 G., Mariash, H., McLennan, D., Rosqvist, G.N., Sato, A., Savela, H., Schneebeli, M., Sokolov, A.,
608 Sokratov, S.A., Terzago, S., Vikhamar-Schuler, D., Williamson, S., Qiu, Y., Callaghan, T.V., 2016.
609 Changing Arctic snow cover: A review of recent developments and assessment of future needs for
610 observations, modelling, and impacts. *Ambio* 45, 516–537. <https://doi.org/10.1007/s13280-016-0770-0>

611 Cayan, D.R., 1996. Interannual Climate Variability and Snowpack in the Western United States. *J. Clim.* 9, 928–
612 948. [https://doi.org/10.1175/1520-0442\(1996\)009<0928:ICVASI>2.0.CO;2](https://doi.org/10.1175/1520-0442(1996)009<0928:ICVASI>2.0.CO;2)

613 Clark, M.P., Nijssen, B., Lundquist, J., Kavetski, D., Rupp, D.E., Woods, R.A., Freer, J.E., Gutmann, E.D., Wood,
614 A.W., Brekke, L.D., Arnold, J.R., Gochis, D.J., Rasmussen, R.M., 2015. A unified approach for process-
615 based hydrologic modeling: 1. Modeling concept. *Water Resour. Res.* 51, 2498–2514.
616 <https://doi.org/10.1002/2015WR017198>

617 Copeland, J.P., McKelvey, K.S., Aubry, K.B., Landa, A., Persson, J., Inman, R.M., Krebs, J., Lofroth, E., Golden,
618 H., Squires, J.R., Magoun, A., Schwartz, M.K., Wilmot, J., Copeland, C.L., Yates, R.E., Kojola, I., May,
619 R., 2010. The bioclimatic envelope of the wolverine (*Gulo gulo*): do climatic constraints limit its
620 geographic distribution? *Can. J. Zool.* 88, 233–246. <https://doi.org/10.1139/Z09-136>

621 Daloz, A.S., Mateling, M., L’Ecuyer, T., Kulie, M., Wood, N.B., Durand, M., Wrzesien, M., Stjern, C.W., Dimri,
622 A.P., 2020. How much snow falls in the world’s mountains? A first look at mountain snowfall estimates in
623 A-train observations and reanalyses. *The Cryosphere* 14, 3195–3207. [https://doi.org/10.5194/tc-14-3195-](https://doi.org/10.5194/tc-14-3195-2020)
624 2020

625 Dierauer, J.R., Allen, D.M., Whitfield, P.H., 2019. Snow Drought Risk and Susceptibility in the Western United
626 States and Southwestern Canada. *Water Resour. Res.* 55, 3076–3091.
627 <https://doi.org/10.1029/2018WR023229>

628 Donald, J.R., Soulis, E.D., Kouwen, N., Pietroniro, A., 1995. A Land Cover-Based Snow Cover Representation for
629 Distributed Hydrologic Models. *Water Resour. Res.* 31, 995–1009. <https://doi.org/10.1029/94WR02973>

630 Dozier, J., 1989. Spectral signature of alpine snow cover from the landsat thematic mapper. *Remote Sens. Environ.*
631 28, 9–22. [https://doi.org/10.1016/0034-4257\(89\)90101-6](https://doi.org/10.1016/0034-4257(89)90101-6)

632 Durner, G.M., Simac, K., Amstrup, S.C., 2013. Mapping Polar Bear Maternal Denning Habitat in the National
633 Petroleum Reserve — Alaska with an IfSAR Digital Terrain Model. *Arctic* 66, 197–206.

634 Egli, L., Jonas, T., Grünwald, T., Schirmer, M., Burlando, P., 2012. Dynamics of snow ablation in a small Alpine
635 catchment observed by repeated terrestrial laser scans. *Hydrol. Process.* 26, 1574–1585.

636 Eyring, V., Bony, S., Meehl, G.A., Senior, C.A., Stevens, B., Stouffer, R.J., Taylor, K.E., 2016. Overview of the
637 Coupled Model Intercomparison Project Phase 6 (CMIP6) experimental design and organization. *Geosci.*
638 *Model Dev.* 9, 1937–1958. <https://doi.org/10.5194/gmd-9-1937-2016>

639 Feng, X., Sahoo, A., Arsenault, K., Houser, P., Luo, Y., Troy, T.J., 2008. The Impact of Snow Model Complexity at
640 Three CLPX Sites. *J. Hydrometeorol.* 9, 1464–1481. <https://doi.org/10.1175/2008JHM860.1>

641 Gelaro, R., McCarty, W., Suárez, M.J., Todling, R., Molod, A., Takacs, L., Randles, C.A., Darmenov, A.,
642 Bosilovich, M.G., Reichle, R., Wargan, K., Coy, L., Cullather, R., Draper, C., Akella, S., Buchard, V.,
643 Conaty, A., Silva, A.M. da, Gu, W., Kim, G.-K., Koster, R., Lucchesi, R., Merkova, D., Nielsen, J.E.,
644 Partyka, G., Pawson, S., Putman, W., Rienecker, M., Schubert, S.D., Sienkiewicz, M., Zhao, B., 2017. The
645 Modern-Era Retrospective Analysis for Research and Applications, Version 2 (MERRA-2). *J. Clim.* 30,
646 5419–5454. <https://doi.org/10.1175/JCLI-D-16-0758.1>

647 Giroto, M., Margulis, S.A., Durand, M., 2014. Probabilistic SWE reanalysis as a generalization of deterministic
648 SWE reconstruction techniques. *Hydrol. Process.* 28, 3875–3895. <https://doi.org/10.1002/hyp.9887>

649 Glass, T.W., Breed, G.A., Liston, G.E., Reinking, A.K., Robards, M.D., Kielland, K., 2021. Spatiotemporally
650 variable snow properties drive habitat use of an Arctic mesopredator. *Oecologia* 195, 887–899.
651 <https://doi.org/10.1007/s00442-021-04890-2>

652 Grünwald, T., Bühler, Y., Lehning, M., 2014. Elevation dependency of mountain snow depth. *The Cryosphere* 8,
653 2381–2394. <https://doi.org/10.5194/tc-8-2381-2014>

654 Hall, D.K., Riggs, G.A., 2007. Accuracy assessment of the MODIS snow products. *Hydrol. Process.* 21, 1534–1547.
655 <https://doi.org/10.1002/hyp.6715>

656 Hamlet, A.F., Mote, P.W., Clark, M.P., Lettenmaier, D.P., 2005. Effects of Temperature and Precipitation
657 Variability on Snowpack Trends in the Western United States. *J. Clim.* 18, 4545–4561.
658 <https://doi.org/10.1175/JCLI3538.1>

659 Harder, P., Pomeroy, J., 2013. Estimating precipitation phase using a psychrometric energy balance method. *Hydrol.*
660 *Process.* 27, 1901–1914. <https://doi.org/10.1002/hyp.9799>

661 Härer, S., Bernhardt, M., Siebers, M., Schulz, K., 2018. On the need for a time- and location-dependent estimation
662 of the NDSI threshold value for reducing existing uncertainties in snow cover maps at different scales. *The*
663 *Cryosphere* 12, 1629–1642. <https://doi.org/10.5194/tc-12-1629-2018>

664 Harpold, A., Dettinger, M., Rajagopal, S., 2017. Defining Snow Drought and Why It Matters. *Eos.*
665 <https://doi.org/10.1029/2017EO068775>

666 He, S., Ohara, N., Miller, S.N., 2019. Understanding subgrid variability of snow depth at 1-km scale using Lidar
667 measurements. *Hydrol. Process.* 33, 1525–1537. <https://doi.org/10.1002/hyp.13415>

668 Helbig, N., Bühler, Y., Eberhard, L., Deschamps-Berger, C., Gascoin, S., Dumont, M., Revuelto, J., Deems, J.S.,
669 Jonas, T., 2021. Fractional snow-covered area: scale-independent peak of winter parameterization. *The*
670 *Cryosphere* 15, 615–632. <https://doi.org/10.5194/tc-15-615-2021>

671 Helbig, N., van Herwijnen, A., Magnusson, J., Jonas, T., 2015. Fractional snow-covered area parameterization over
672 complex topography. *Hydrol. Earth Syst. Sci.* 19, 1339–1351. <https://doi.org/10.5194/hess-19-1339-2015>

673 Heldmyer, A.J., Bjarke, N.R., Livneh, B., 2023. A 21st-Century perspective on snow drought in the Upper Colorado
674 River Basin. *JAWRA J. Am. Water Resour. Assoc.* 59, 396–415. <https://doi.org/10.1111/1752-1688.13095>

675 Herman, J.D., Giuliani, M., 2018. Policy tree optimization for threshold-based water resources management over
676 multiple timescales. *Environ. Model. Softw.* 99, 39–51. <https://doi.org/10.1016/j.envsoft.2017.09.016>

677 Inman, R.M., Magoun, A.J., Persson, J., Mattisson, J., 2012. The wolverine’s niche: linking reproductive
678 chronology, caching, competition, and climate. *J. Mammal.* 93, 634–644. [https://doi.org/10.1644/11-
680 MAMM-A-319.1](https://doi.org/10.1644/11-

679 MAMM-A-319.1)

680 Jennings, K.S., Winchell, T.S., Livneh, B., Molotch, N.P., 2018. Spatial variation of the rain–snow temperature
681 threshold across the Northern Hemisphere. *Nat. Commun.* 9, 1148. [https://doi.org/10.1038/s41467-018-
683 03629-7](https://doi.org/10.1038/s41467-018-

682 03629-7)

683 Jonas, T., Marty, C., Magnusson, J., 2009. Estimating the snow water equivalent from snow depth measurements in
684 the Swiss Alps. *J. Hydrol.* 378, 161–167. <https://doi.org/10.1016/j.jhydrol.2009.09.021>

685 Kwadijk, J.C.J., Haasnoot, M., Mulder, J.P.M., Hoogvliet, M.M.C., Jeuken, A.B.M., van der Krogt, R.A.A., van
686 Oostrom, N.G.C., Schelfhout, H.A., van Velzen, E.H., van Waveren, H., de Wit, M.J.M., 2010. Using
687 adaptation tipping points to prepare for climate change and sea level rise: a case study in the Netherlands.
688 *WIREs Clim. Change* 1, 729–740. <https://doi.org/10.1002/wcc.64>

689 Laliberte, A.S., Ripple, W.J., 2004. Range Contractions of North American Carnivores and Ungulates. *BioScience*
690 54, 123–138. [https://doi.org/10.1641/0006-3568\(2004\)054\[0123:RCONAC\]2.0.CO;2](https://doi.org/10.1641/0006-3568(2004)054[0123:RCONAC]2.0.CO;2)

691 Liston, G.E., 2004. Representing Subgrid Snow Cover Heterogeneities in Regional and Global Models. *J. Clim.* 17,
692 1381–1397. [https://doi.org/10.1175/1520-0442\(2004\)017<1381:RSSCHI>2.0.CO;2](https://doi.org/10.1175/1520-0442(2004)017<1381:RSSCHI>2.0.CO;2)

693 Liston, G.E., Elder, K., 2006. A Distributed Snow-Evolution Modeling System (SnowModel). *J. Hydrometeorol.* 7,
694 1259–1276. <https://doi.org/10.1175/JHM548.1>

695 Liston, G.E., Perham, C.J., Shideler, R.T., Chevront, A.N., 2016. Modeling snowdrift habitat for polar bear dens.
696 *Ecol. Model.* 320, 114–134. <https://doi.org/10.1016/j.ecolmodel.2015.09.010>

697 Liu, Y., Margulis, S.A., 2019. Deriving Bias and Uncertainty in MERRA-2 Snowfall Precipitation Over High
698 Mountain Asia. *Front. Earth Sci.* 7. <https://doi.org/10.3389/feart.2019.00280>

699 Livneh, B., Deems, J.S., Schneider, D., Barsugli, J.J., Molotch, N.P., 2014. Filling in the gaps: Inferring spatially
700 distributed precipitation from gauge observations over complex terrain. *Water Resour. Res.* 50, 8589–8610.
701 <https://doi.org/10.1002/2014WR015442>

702 Luce, C.H., Tarboton, D.G., Cooley, K.R., 1998. The influence of the spatial distribution of snow on basin-averaged
703 snowmelt. *Hydrol. Process.* 12, 1671–1683. [https://doi.org/10.1002/\(SICI\)1099-
705 1085\(199808/09\)12:10/11<1671::AID-HYP688>3.0.CO;2-N](https://doi.org/10.1002/(SICI)1099-

704 1085(199808/09)12:10/11<1671::AID-HYP688>3.0.CO;2-N)

705 Lundquist, J.D., Dettinger, M.D., 2005. How snowpack heterogeneity affects diurnal streamflow timing. *Water*
706 *Resour. Res.* 41. <https://doi.org/10.1029/2004WR003649>

707 Machguth, H., Paul, F., Hoelzle, M., Haerberli, W., 2006. Distributed glacier mass-balance modelling as an
708 important component of modern multi-level glacier monitoring. *Ann. Glaciol.* 43, 335–343.
709 <https://doi.org/10.3189/172756406781812285>

710 Magoun, A.J., Robards, M.D., Packila, M.L., Glass, T.W., 2017. Detecting snow at the den-site scale in wolverine
711 denning habitat. *Wildl. Soc. Bull.* 41, 381–387. <https://doi.org/10.1002/wsb.765>

712 Maher, A.I., Treitz, P.M., Ferguson, M.A.D., 2012. Can Landsat data detect variations in snow cover within habitats
713 of arctic ungulates? *Wildl. Biol.* 18, 75–87. <https://doi.org/10.2981/11-055>

714 Mahoney, P.J., Liston, G.E., LaPoint, S., Gurarie, E., Mangipane, B., Wells, A.G., Brinkman, T.J., Eitel, J.U.H.,
715 Hebblewhite, M., Nolin, A.W., Boelman, N., Prugh, L.R., 2018. Navigating snowscapes: scale-dependent
716 responses of mountain sheep to snowpack properties. *Ecol. Appl.* 28, 1715–1729.
717 <https://doi.org/10.1002/eap.1773>

718 Margulis, S.A., Cortés, G., Giroto, M., Durand, M., 2016. A Landsat-Era Sierra Nevada Snow Reanalysis (1985–
719 2015). *J. Hydrometeorol.* 17, 1203–1221. <https://doi.org/10.1175/JHM-D-15-0177.1>

720 Margulis, S.A., Giroto, M., Cortés, G., Durand, M., 2015. A Particle Batch Smoother Approach to Snow Water
721 Equivalent Estimation. *J. Hydrometeorol.* 16, 1752–1772. <https://doi.org/10.1175/JHM-D-14-0177.1>

722 Margulis, S.A., Liu, Y., Baldo, E., 2019. A Joint Landsat- and MODIS-Based Reanalysis Approach for Midlatitude
723 Montane Seasonal Snow Characterization. *Front. Earth Sci.* 7. <https://doi.org/10.3389/feart.2019.00272>

724 McKelvey, K.S., Copeland, J.P., Schwartz, M.K., Littell, J.S., Aubry, K.B., Squires, J.R., Parks, S.A., Elsner, M.M.,
725 Mauger, G.S., 2011. Climate change predicted to shift wolverine distributions, connectivity, and dispersal
726 corridors. *Ecol. Appl.* 21, 2882–2897. <https://doi.org/10.1890/10-2206.1>

727 Mendoza, P.A., Musselman, K.N., Revuelto, J., Deems, J.S., López-Moreno, J.I., McPhee, J., 2020. Interannual and
728 Seasonal Variability of Snow Depth Scaling Behavior in a Subalpine Catchment. *Water Resour. Res.* 56,
729 e2020WR027343. <https://doi.org/10.1029/2020WR027343>

730 Mote, P.W., Hamlet, A.F., Clark, M.P., Lettenmaier, D.P., 2005. DECLINING MOUNTAIN SNOWPACK IN
731 WESTERN NORTH AMERICA*. *Bull. Am. Meteorol. Soc.* 86, 39–50. <https://doi.org/10.1175/BAMS-86-1-39>

732

733 Nolin, A.W., Daly, C., 2006. Mapping “at risk” snow in the Pacific Northwest. *J. Hydrometeorol.* 7, 1164–1171.

734 Pestana, S., Chickadel, C.C., Harpold, A., Kostadinov, T.S., Pai, H., Tyler, S., Webster, C., Lundquist, J.D., 2019.
735 Bias Correction of Airborne Thermal Infrared Observations Over Forests Using Melting Snow. *Water*
736 *Resour. Res.* 55, 11331–11343. <https://doi.org/10.1029/2019WR025699>

737 Pflug, J.M., Hughes, M., Lundquist, J.D., 2021. Downscaling snow deposition using historic snow depth patterns:
738 Diagnosing limitations from snowfall biases, winter snow losses, and interannual snow pattern
739 repeatability. *Water Resour. Res.* e2021WR029999. <https://doi.org/10.1029/2021WR029999>

740 Pflug, J.M., Liston, G.E., Nijssen, B., Lundquist, J.D., 2019. Testing Model Representations of Snowpack Liquid
741 Water Percolation Across Multiple Climates. *Water Resour. Res.* 55, 4820–4838.
742 <https://doi.org/10.1029/2018WR024632>

743 Pflug, J.M., Lundquist, J.D., 2020. Inferring Distributed Snow Depth by Leveraging Snow Pattern Repeatability:
744 Investigation Using 47 Lidar Observations in the Tuolumne Watershed, Sierra Nevada, California. *Water*
745 *Resour. Res.* 56, e2020WR027243. <https://doi.org/10.1029/2020WR027243>

746 Pflug, J.M., Margulis, S.A., Lundquist, J.D., 2022. Inferring watershed-scale mean snowfall magnitude and
747 distribution using multidecadal snow reanalysis patterns and snow pillow observations. *Hydrol. Process.*
748 36, e14581. <https://doi.org/10.1002/hyp.14581>

749 Ray, A.L., Barsugli, J.J., Livneh, B., Dewes, C.F., Rangwala, I., Heldmyer, A., Stewart, J., 2017. Future Snow
750 Persistence in Rocky Mountain and Glacier National Parks: An Analysis to Inform the USFWS Wolverine
751 Species Status Assessment. NOAA/ESRL/Physical Sciences Division, CU/Cooperative Institute for
752 Research in Environmental Sciences (CIRES), and CU Civil, Environmental & Architectural Engineering.

753 Sankey, T., Donald, J., McVay, J., Ashley, M., O’Donnell, F., Lopez, S.M., Springer, A., 2015. Multi-scale analysis
754 of snow dynamics at the southern margin of the North American continental snow distribution. *Remote*
755 *Sens. Environ.* 169, 307–319. <https://doi.org/10.1016/j.rse.2015.08.028>

756 Scott, J.D., Alexander, M.A., Murray, D.R., Swales, D., Eischeid, J., 2016. The Climate Change Web Portal: A
757 System to Access and Display Climate and Earth System Model Output from the CMIP5 Archive. *Bull.*
758 *Am. Meteorol. Soc.* 97, 523–530. <https://doi.org/10.1175/BAMS-D-15-00035.1>

759 Serreze, M.C., Clark, M.P., Armstrong, R.L., McGinnis, D.A., Pulwarty, R.S., 1999. Characteristics of the western
760 United States snowpack from snowpack telemetry (SNO_{TEL}) data. *Water Resour. Res.* 35, 2145–2160.
761 <https://doi.org/10.1029/1999WR900090>

762 Shih, J.-S., ReVelle, C., 1995. Water supply operations during drought: A discrete hedging rule. *Eur. J. Oper. Res.*
763 82, 163–175. [https://doi.org/10.1016/0377-2217\(93\)E0237-R](https://doi.org/10.1016/0377-2217(93)E0237-R)

764 Sivy, K.J., Nolin, A.W., Cosgrove, C.L., Prugh, L.R., 2018. Critical snow density threshold for Dall’s sheep (*Ovis*
765 *dalli dalli*). *Can. J. Zool.* 96, 1170–1177. <https://doi.org/10.1139/cjz-2017-0259>

766 Skaugen, T., Melvold, K., 2019. Modeling the Snow Depth Variability With a High-Resolution Lidar Data Set and
767 Nonlinear Terrain Dependency. *Water Resour. Res.* 55, 9689–9704.
768 <https://doi.org/10.1029/2019WR025030>

769 USFWS, 2018. Species status assessment report for the North American Wolverine (*Gulo gulo luscus*). (No. Version
770 1.2.). U.S. Fish and Wildlife Service, Mountain-Prarie Region, Lakewood, CO.
771 Vögeli, C., Lehning, M., Wever, N., Bavay, M., 2016. Scaling Precipitation Input to Spatially Distributed
772 Hydrological Models by Measured Snow Distribution. *Front. Earth Sci.* 4.
773 <https://doi.org/10.3389/feart.2016.00108>
774 Wayand, N.E., Clark, M.P., Lundquist, J.D., 2017. Diagnosing snow accumulation errors in a rain-snow transitional
775 environment with snow board observations. *Hydrol. Process.* 31, 349–363.
776 <https://doi.org/10.1002/hyp.11002>
777 Wigmosta, M.S., Nijssen, B., Storck, P., Lettenmaier, D.P., 2002. The distributed hydrology soil vegetation model.
778 *Math. Models Small Watershed Hydrol. Appl.* 7–42.
779 Xiao, M., Mahanama, S.P., Xue, Y., Chen, F., Lettenmaier, D.P., 2021. Modeling Snow Ablation over the
780 Mountains of the Western United States: Patterns and Controlling Factors. *J. Hydrometeorol.* 22, 297–311.
781 <https://doi.org/10.1175/JHM-D-19-0198.1>
782 Xue, Y., Sellers, P.J., Kinter, J.L., Shukla, J., 1991. A Simplified Biosphere Model for Global Climate Studies. *J.*
783 *Clim.* 4, 345–364. [https://doi.org/10.1175/1520-0442\(1991\)004<0345:ASBMFG>2.0.CO;2](https://doi.org/10.1175/1520-0442(1991)004<0345:ASBMFG>2.0.CO;2)
784 Yang, K., Musselman, K.N., Rittger, K., Margulis, S.A., Painter, T.H., Molotch, N.P., 2021. Combining ground-
785 based and remotely sensed snow data in a linear regression model for real-time estimation of snow water
786 equivalent. *Adv. Water Resour.* 104075. <https://doi.org/10.1016/j.advwatres.2021.104075>
787